

The effects of manufacturing variability on turbine vane performance

by

John D. Duffner

B.S., Aerospace Engineering (2006)

University of Notre Dame

Submitted to the Department of Aeronautics and Astronautics
in partial fulfillment of the requirements for the degree of

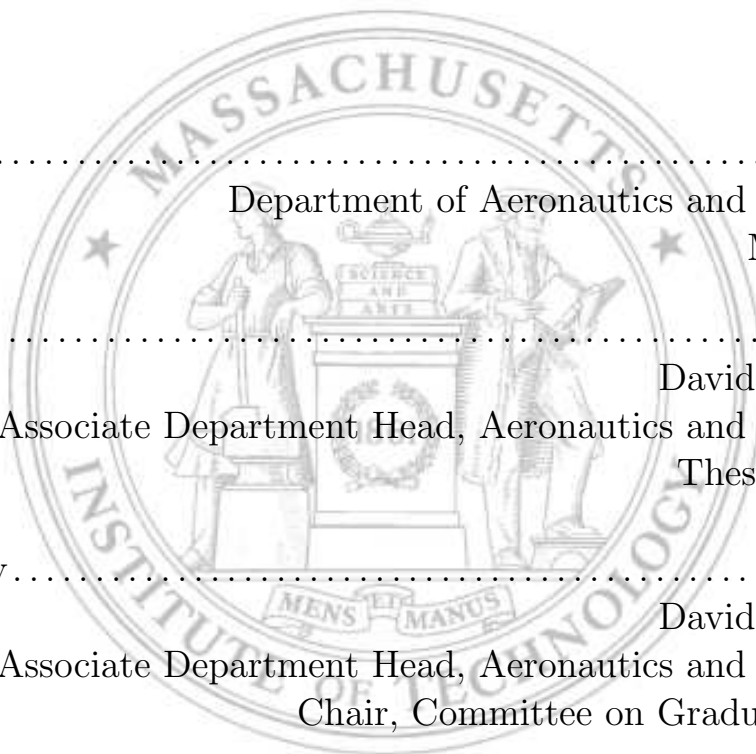
Master of Science in Aerospace Engineering

at the

MASSACHUSETTS INSTITUTE OF TECHNOLOGY

June 2008

© Massachusetts Institute of Technology 2008. All rights reserved.



Author
Department of Aeronautics and Astronautics
May 30, 2008

Certified by
David L. Darmofal
Associate Department Head, Aeronautics and Astronautics
Thesis Supervisor

Accepted by
David L. Darmofal
Associate Department Head, Aeronautics and Astronautics
Chair, Committee on Graduate Students

The effects of manufacturing variability on turbine vane performance

by
John D. Duffner

Submitted to the Department of Aeronautics and Astronautics
on May 30, 2008, in partial fulfillment of the
requirements for the degree of
Master of Science in Aerospace Engineering

Abstract

Gas turbine vanes have airfoil shapes optimized to deliver specific flow conditions to turbine rotors. The limitations of the manufacturing process with regards to accuracy and precision mean that no vane will exactly match the design intent. This research effort is an investigation of the effects of manufacturing-induced geometry variability on the performance of a transonic turbine vane. Variability is characterized by performing Principal Components Analysis (PCA) on a set of measured vanes and then applied to a different vane design. The performance scatter of that design is estimated through Monte Carlo analysis. The effect of a single PCA mode on performance is estimated and it is found that some modes with lower geometric variability can have greater impact on performance metrics. Linear sensitivity analysis, both viscous and inviscid, is carried out to survey performance sensitivity to localized surface perturbations, and tolerances are evaluated using these results. The flow field is seen to be practically insensitive to shape changes upstream of the throat. Especially sensitive locations like the throat and trailing edge are investigated further through nonlinear sensitivity analysis.

Thesis Supervisor: David L. Darmofal

Title: Associate Department Head, Aeronautics and Astronautics

Acknowledgments

Completing this work has placed me gladly in the debt of many who have helped me get to and through MIT. Prof. Dave Darmofal's insight and patience have been instrumental in improving both this thesis and the student who wrote it. I consider myself fortunate to have been the beneficiary of his guidance.

I am thankful to Prof. Mark Drela for creating MISES and for supporting it by answering my numerous questions. Similarly I would like to thank the ProjectX team, particularly Garrett Barter, J.M. Modisette, and Todd Oliver, for all their help. The wisdom and kind assistance of Prof. Rob Miller are also much appreciated.

I owe a debt of gratitude to Rolls-Royce for establishing the Sir Frank Whittle Fellowship which provided the means for me to realize my dream of attending MIT. Additionally, the company provided invaluable data and the expertise of Dr. Steve Gegg, Eugene Clemens, and Ed Turner.

I would not trade my time at MIT for anything, although it has been difficult at times. I've been lucky to have had some very good people to lean on for support and balance. My roommates and the varsity crew team helped my well-being immeasurably.

Most of all, I must thank my family for their support throughout this work and throughout my life. Their encouragement and sacrifices on my behalf are the ultimate source of all of my accomplishments.

This work was supported by funding from Rolls-Royce.

Contents

1	Introduction	11
1.1	Motivation	11
1.2	Objectives	13
1.3	Approach	13
1.4	Organization	14
2	Geometric Analysis	15
2.1	Blade Measurement Process	15
2.2	Principal Components Analysis	16
2.2.1	Methods	16
2.2.2	Results	18
2.3	Vane Generation	27
3	CFD Analysis	29
3.1	Performance Scatter of Generated Vanes	29
3.1.1	Methods	29
3.1.2	Results	31
3.2	Sensitivity to PCA Modes	35
3.3	Sensitivity to Localized Bump Perturbations	39
3.3.1	Linear Sensitivity in MISES	39
3.3.2	Nonlinear Sensitivity Analysis	51
4	Comparison with Discontinuous-Galerkin Sensitivity Results	57
4.1	Methods	57
4.2	Results	61
5	Summary and Conclusions	67
5.1	Suggestions for Future Work	68
	Bibliography	70

List of Figures

2-1	Turbine vane doublet.	18
2-2	Quantile-quantile plots of PCA mode amplitude.	20
2-3	Scatter fraction of PCA modes.	22
2-4	Dominant modes, leading airfoil.	23
2-5	Dominant modes, leading airfoil.	24
2-6	Dominant modes, trailing airfoil.	25
2-7	Dominant modes, trailing airfoil.	26
3-1	Distributions of performance quantities.	32
3-2	Inviscid and viscous loss coefficients of the generated vane population.	34
3-3	Sensitivity to dominant PCA modes, leading airfoil.	36
3-4	Sensitivity to dominant PCA modes, trailing airfoil.	37
3-5	Hicks-Henne bump function used to perturb airfoil geometry.	40
3-6	Linear sensitivity results from viscous MISES calculations.	42
3-7	Normal-vector representation of viscous MISES linear sensitivity derivatives.	43
3-8	Sensitivity derivatives compared with Mach contours.	45
3-9	Tolerance bands for specified performance limits.	48
3-10	Linear sensitivity results from inviscid MISES calculations.	49
3-11	Normal-vector representation of inviscid MISES linear sensitivity derivatives.	50
3-12	Locations at which nonlinear sensitivity is investigated.	52
3-13	Nonlinear sensitivity results.	53
3-14	Comparison of inlet Mach number sensitivity.	55
4-1	Nominal grid for DG cases.	59
4-2	Linear sensitivity calculated via DG method.	61
4-3	Comparison of linear sensitivity results.	62
4-4	MISES and DG Mach contours (nominal).	64
4-5	MISES and DG Mach contours. (node 2 perturbed)	65
4-6	MISES and DG Mach contours (node 68 perturbed).	66

Chapter 1

Introduction

1.1 Motivation

The turbine is the source of a gas turbine engine's power as well as many of its technical challenges. The trend of operating at ever higher temperatures, perhaps the most significant tendency in the ongoing development of the jet engine, is almost entirely dependent on the performance of the turbine and its ability to withstand such temperatures[18][25]. It is no surprise then that the gas turbine industry exerts considerable effort on improving turbines.

A turbine consists of one or more stages, each with a row of stationary vanes followed by a rotor immediately downstream. Turbine vanes are designed to condition the airflow for the rotor. They accept flow from the combustor or a preceding stage and give it a tangential swirl which is subsequently taken out or redirected by the rotor. Their airfoil shapes are optimized to impart specified levels of turning and acceleration with minimum loss generation. A transonic vane row may form convergent-divergent passages which accelerate a subsonic inflow to a supersonic outflow at the proper flow rate and angle to match the downstream blade row. Suboptimal performance in the vane row can decrease the amount of work that is extracted in the rotor both directly, by introducing losses, and indirectly, by supplying the rotor with incorrectly-conditioned flow which will cause its efficiency to drop.

Geometry deviations from an optimized airfoil shape naturally lead it to function less than optimally. There are multiple ways in which this can occur. Shifting the trailing edge can cause the turning angle to take on a different value. Over the bulk of the surface, adding or subtracting material changes the cascade passage area which controls flow acceleration and flow rate. If the vane is transonic, any bumps in the region of supersonic flow can potentially cause shocks.

Every manufacturing process has limited accuracy and precision, so products do not exactly match the design intent or each other. There are several processes in the fabrication of a turbine vane: casting, machining, and the application of protective coatings[14]. Each one can and does introduce shape variability, necessitating the use of quality control methods such as tolerancing schemes. Such measures make production more expensive but mitigate the costs associated with putting faulty products into service, such as increased maintenance, recalls, and loss of customers. The successful engine manufacturer must find the appropriate level of tolerancing so as to provide acceptable quality without excessive manufacturing costs. To inform this decision with regards to turbine vanes, one needs an estimate of how their performance is affected by shape variability, which must seek to address the following questions:

- What kind and degree of geometric variability is to be expected, and what is the resulting performance distribution?
- Are there any regions on the vane in which shape deviations have an especially large effect on the vane's performance?
- How tight must the geometric tolerances be to ensure acceptable performance?

The third question represents the manufacturer's decision, which can only be made once the first two questions have been answered. If the engine or a close variant are in production already, manufacturing variability and the consequences thereof can be measured directly and tolerances adjusted accordingly. Estimation is required in the case of a new engine, motivated by the need to ensure that improved designs do

not outpace the capability of the manufacturing process to reliably produce them. The desire to ensure a successful engine model launch places a premium on effective manufacturing and quality control processes.

1.2 Objectives

Put simply, the aim of this research is to estimate how far a manufactured vane is likely to deviate from the design intent and to investigate what causes it to do so. This can be expressed in the form of specific individual goals:

- Characterize the manufacturing variability in a set of manufactured vanes in terms of local shape deviations from the nominal design, and devise a way to apply the observed variability to a new vane design.
- Calculate the expected performance scatter of a manufactured population of the new vanes and estimate the probability that a vane's performance will lie within an acceptable range.
- Quantitatively assess the surface-wise distribution of flow sensitivity to geometric perturbations and use this to evaluate tolerance levels.

1.3 Approach

The objectives are accomplished in the following manner. Principal Components Analysis is performed on vane measurement data provided by Rolls-Royce. In this way the manufacturing variability in one radial section is decomposed into a set of mode shapes. A set of new vanes, with a different nominal design than those measured, is then generated using random combinations of these modes. The combinations account for the fact that each mode is responsible for a different share of the observed geometric scatter and thus each has a different likelihood of being expressed to a significant degree. In order for the measured variability to be applied to the generated vanes, each mode

is represented in terms of normal displacement as a function of arc length along the vane's surface.

The performance of these vanes is estimated using the inviscid-viscous coupled flow model MISES[9]. The performance distribution of the generated population is compared to the nominal values and evaluated against specified limits. The performance effects of individual dominant modes is determined; combined with the probability distribution of mode shape amplitudes, this makes it possible to estimate the probability that a random manufactured vane will non-conform.

The flow field's sensitivity to geometry perturbation is investigated in an effort to locate the sources of the estimated performance scatter. Linear sensitivity analysis is carried out by applying localized bump modes all along the surface of the vane. MISES enables direct calculation of sensitivity derivatives with respect to virtual bump mode amplitude for both viscous and inviscid cases. A discontinuous-Galerkin solver (the MIT-developed ProjectX[11][10][22]) is used to provide a check on the trends and magnitudes of the inviscid sensitivity derivatives. The viscous MISES derivatives are used in conjunction with specified performance limits to convert the sensitivity behavior into geometric tolerances. Nonlinear sensitivity analysis is performed using MISES in regions that are identified by the linear analysis as being particularly sensitive. This is done by introducing a series of finite displacements from the nominal shape.

1.4 Organization

The remainder of this thesis is organized in the following manner. Chapter 2 details the geometric analysis used to characterize the manufacturing variability and generate new vanes. The third chapter describes the CFD results for performance scatter and flow sensitivity to shape perturbations. Chapter 4 presents alternative sensitivity results for comparison to those in the previous chapter, and Chapter 5 contains concluding remarks and suggestions for follow-on work.

Chapter 2

Geometric Analysis

The impact of manufacturing variability on vane performance begins with modeling the geometry perturbations. Specifically, the following steps are taken:

1. Take geometric measurements (at one radial section) of a set of manufactured turbine vanes.
2. Perform Principal Components Analysis (PCA) on the measured geometry data.
3. Generate a probabilistically accurate set of vanes according to the geometry perturbation modes described by PCA.

2.1 Blade Measurement Process

The raw geometry data which forms the basis of the performance scatter estimate is collected using a Coordinate Measuring Machine (CMM). The machine uses a stylus to physically measure the location of an object's surface. For this study, the measurements are taken at a radial location corresponding to the midspan of the vane. The measured population consists of 25 vane doublets, i.e., each manufactured part has two vane airfoils. The typical CMM output contains 700 to 800 measured coordinate pairs. This is many more points than are included in the nominal design definition to which the data is compared. Therefore the data set is truncated by matching

each design point with the closest measured point so that there can be a one-to-one correspondence between the nominal definition and each measured blade shape.

2.2 Principal Components Analysis

2.2.1 Methods

Principal Components Analysis is used in this work to quantitatively characterize the observed manufacturing-induced shape variability[12][13][19]. This allows one to grow a relatively small measured vane population into a larger, randomly generated population with the same variability, thus enabling performance evaluation of a large set of vanes without having to actually manufacture them. The ability to do this without real vanes is particularly important to this analysis, in which the variability seen in an existing vane design (referred to hereafter as Type I) is applied to a proposed design (Type II) of which no examples have yet been made.

Garzon[12][13] describes the workings and use of PCA, and his description will be summarized here. As implemented in this work, PCA separates a set of measured geometries into the mean geometry \bar{x} and a set of m perturbation modes v_i . The number of modes m is equal to the number of points in each measured geometry, but only $N - 1$ of them have nonzero scatter fractions, where N is the number of blades in the measured set. The j^{th} measured blade \hat{x}_j can thus be described by Equation 2.1 below. Note that in this context, x and v represent 2-dimensional geometry, not just the x-coordinate.

$$\hat{x}_j = \bar{x} + \sum_{i=1}^m a_{ij}v_i \quad (2.1)$$

Each measured blade is therefore the sum of the average blade with a weighted sum of the modal perturbations. As mentioned in Section 2.1, the measured data points that are considered in PCA are those that most closely correspond to the nominal definition points. The mode shapes and their amplitudes are calculated by taking the Singular Value Decomposition (SVD) of a matrix X , each row of which is a vector

describing the pointwise deviation from the nominal in a single measured blade. The SVD is given as follows:

$$X = U\Sigma V^T \quad (2.2)$$

in which Σ is diagonal with its nonzero elements equal to the square root of the eigenvalues of X 's scatter matrix S :

$$S = X^T X \quad (2.3)$$

The eigenvalues of S correspond to the variances of the mode amplitudes. The columns of V are the eigenvectors of S , which correspond to the modal geometries v , and U contains the contribution of each perturbation mode to the geometry of each measured blade. The variance of each mode amplitude, when divided by the sum of all the variances, represents the scatter fraction of that mode, which is its contribution to the total geometric variability of the measured population. A compact SVD is used instead of a full one; this outputs only the modes with nonzero scatter fraction.

The mold used to produce a doublet cannot guarantee identical airfoil shapes. For this reason, the measurement data is segregated into two distinct populations, one for the leading or #1 airfoil and one for the trailing or #2 airfoil in the doublet (see Figure 2-1). Generation of perturbed blades is also done separately based on the PCA output of each population.

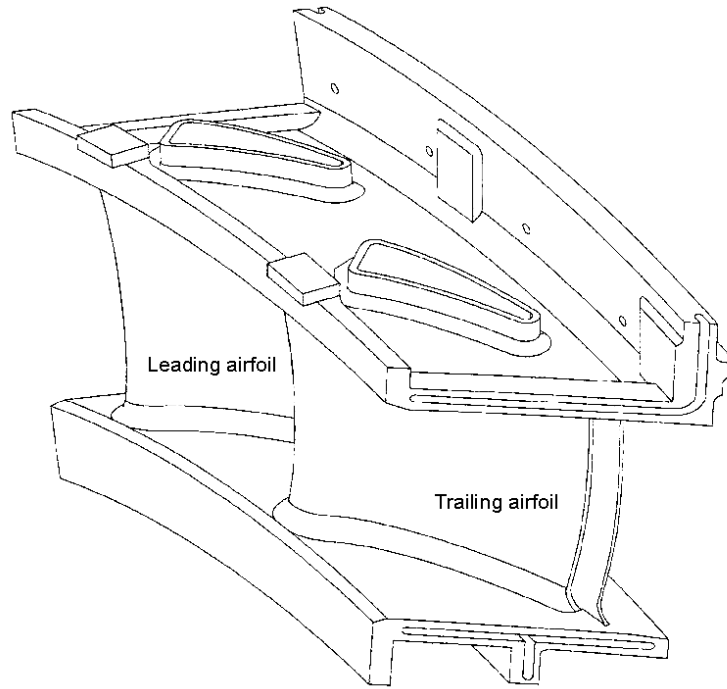


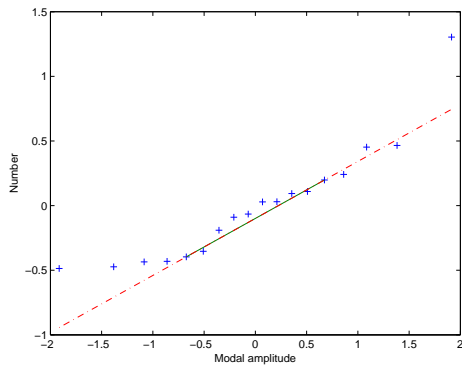
Figure 2-1: Turbine vane doublet[14].

For a much more comprehensive discussion of Principal Components Analysis in an aerodynamic design context, the reader is referred to Chapter 2 and Appendix A of Garzon[12].

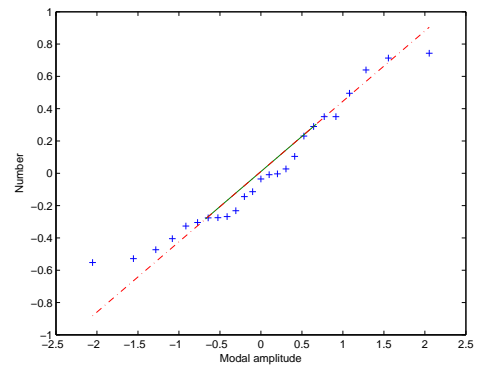
2.2.2 Results

The measured Type I vane population consists of 25 vane doublets. However for the leading airfoil, only 18 are included in the PCA analysis since 7 of the leading airfoils have been intentionally notched on the trailing edge to indicate that those doublets are to be scrapped (for reasons unrelated to geometric shape tolerances). Since this notch introduces a shape change far more severe than any that could normally be caused by the manufacturing process, the leading airfoils of the scrapped doublets cannot be included in the PCA calculations, else they would greatly skew the resulting modes. For this reason the leading airfoil has only 17 PCA modes.

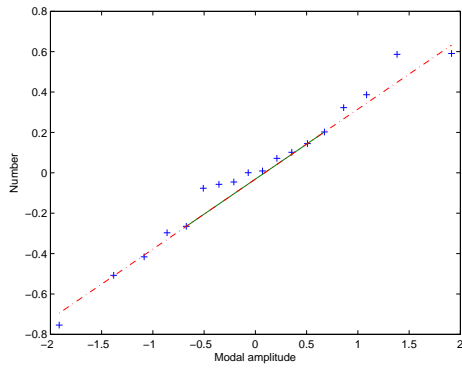
The nature of the distribution of the mode shape amplitudes within the measured population is important for the generation of a statistically-accurate set of new vanes. The validity of the assumption that the mode shape amplitudes are normally distributed is checked using a Kolmogorov-Smirnov test[24]. In this population, that assumption is a valid one according to a Kolmogorov-Smirnov test at the 95% level. Quantile-quantile plots for the first three PCA modes of each airfoil are given in Figure 2-2. The p -values from the K-S test are tabulated in Table 2.1. The p -value is the probability of obtaining the observed data assuming that the mode shape amplitudes follow a standard normal distribution[27]. The lower the value, the less likely it is that the standard normal distribution is an suitable fit.



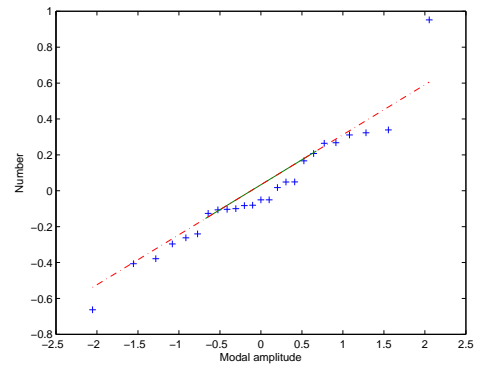
(a) Leading airfoil, mode 1



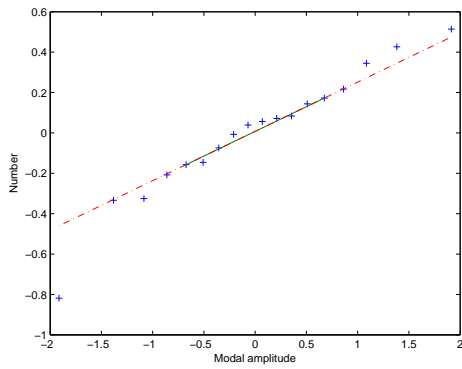
(b) Trailing airfoil, mode 1



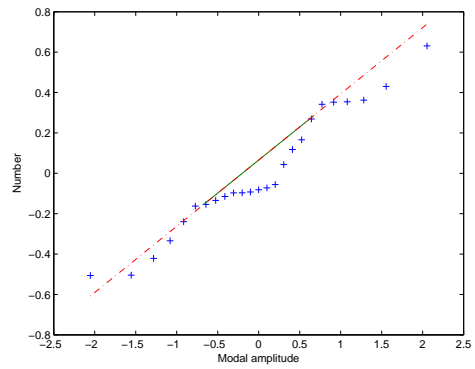
(c) Leading airfoil, mode 2



(d) Trailing airfoil, mode 2



(e) Leading airfoil, mode 3



(f) Trailing airfoil, mode 3

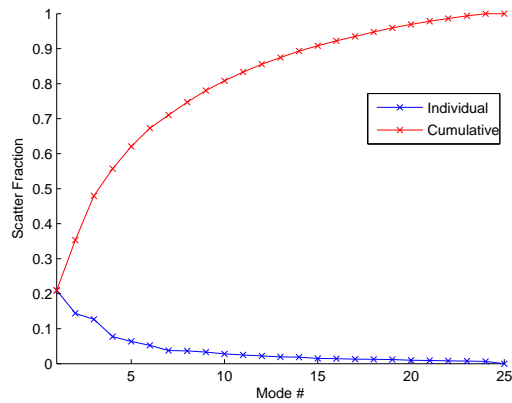
Figure 2-2: Quantile-quantile plots of PCA mode amplitude.

Mode	p -value (Leading Airfoil)	p -value (Trailing Airfoil)
1	0.853	0.801
2	0.856	0.822
3	0.983	0.404
4	0.953	0.412
5	0.984	0.808
6	0.564	0.999
7	0.820	0.643
8	0.989	0.870
9	0.784	0.959
10	0.967	0.820
11	0.984	0.319
12	0.999	0.938
13	0.576	0.660
14	0.967	0.834
15	0.713	0.837
16	0.959	0.796
17	1.000	0.516
18	N/A	0.872
19	N/A	0.556
20	N/A	0.863
21	N/A	0.349
22	N/A	0.325
23	N/A	0.918
24	N/A	0.787

Table 2.1: K-S test p -values

The scatter fraction of the PCA modes is as follows:

(a) Leading airfoil

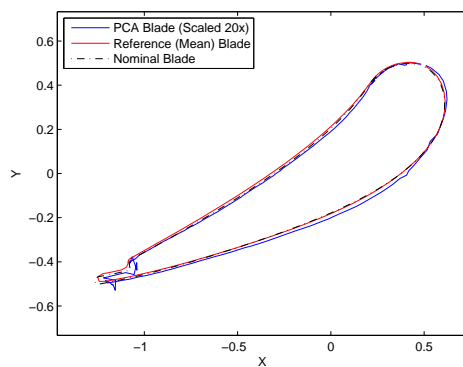


(b) Trailing airfoil

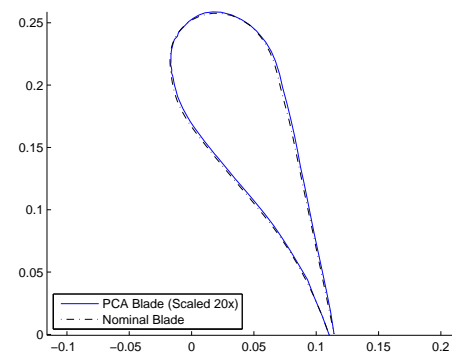
Figure 2-3: Scatter fraction of PCA modes.

As evidenced by the above plots, a relative handful of modes is responsible for the bulk of the geometric variability observed in the Type I population. There is practically no additional cost for including all of them when generating new blades, but their relative dominance can inform the manufacturer as to where the fabrication process most needs to be improved. Some of the dominant modes are shown in Figures

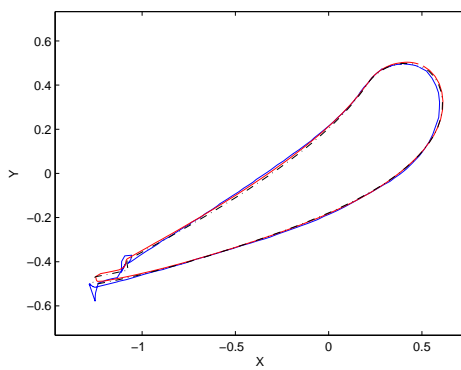
2-4 through 2-7, both as observed in the Type I population and as applied to the Type II vane. Modes are ordered according to their scatter fraction: the lower a mode's number, the more likely it is to find significant expression in a manufactured vane. Note that although positive-amplitude modes are displayed here, they are just as likely to be negative in the measured and generated populations.



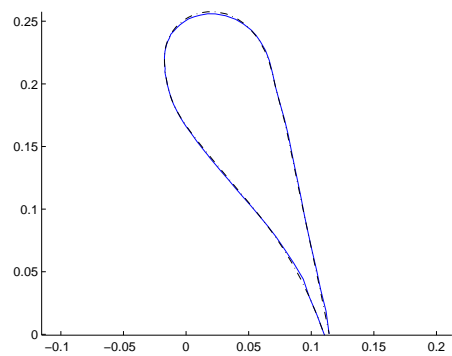
(a) Mode 1 on Type I



(b) Mode 1 on Type II

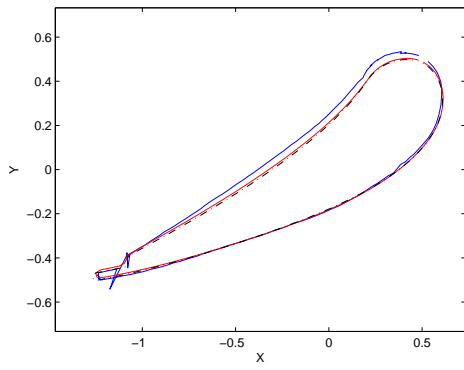


(c) Mode 2 on Type I

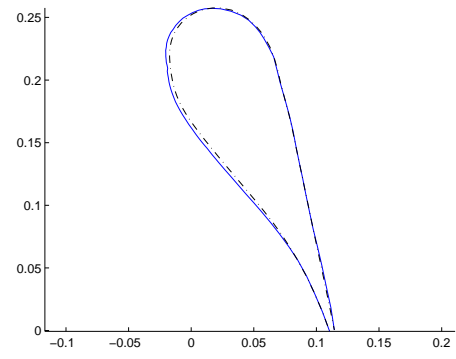


(d) Mode 2 on Type II

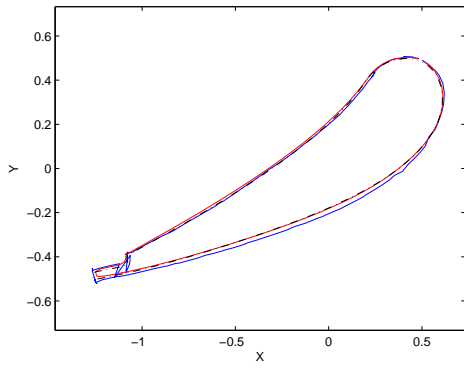
Figure 2-4: Dominant modes, leading airfoil.



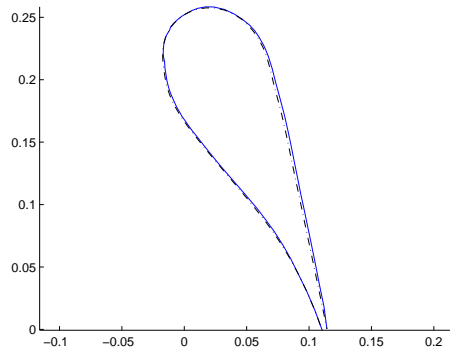
(a) Mode 3 on Type I



(b) Mode 3 on Type II

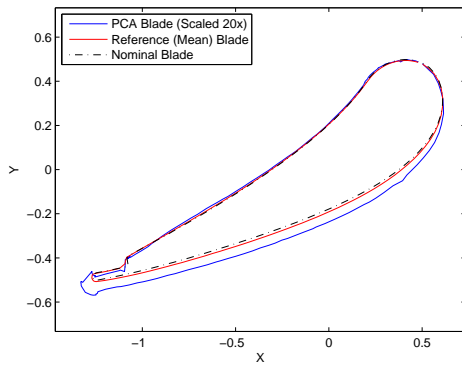


(c) Mode 4 on Type I

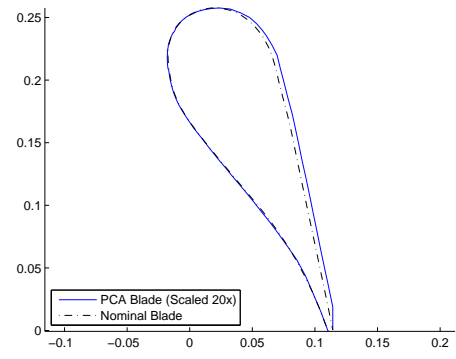


(d) Mode 4 on Type II

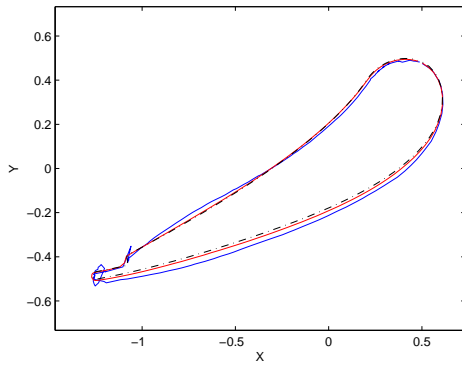
Figure 2-5: Dominant modes, leading airfoil.



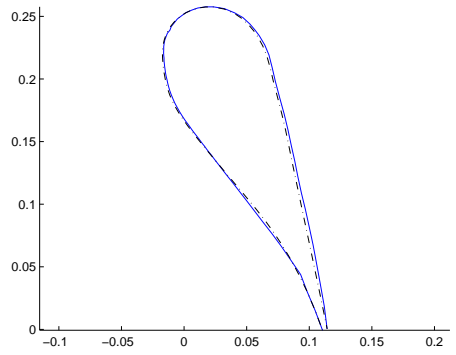
(a) Mode 1 on Type I



(b) Mode 1 on Type II

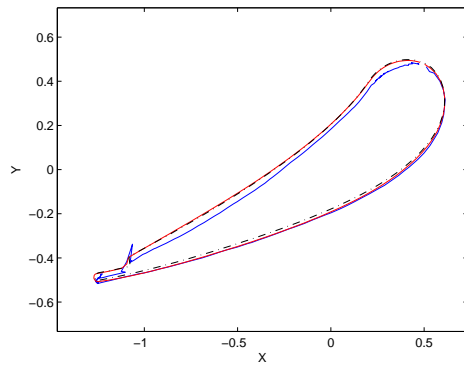


(c) Mode 2 on Type I

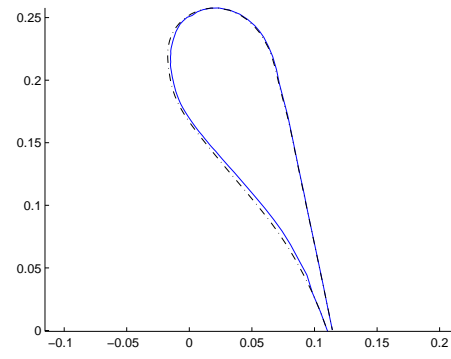


(d) Mode 2 on Type II

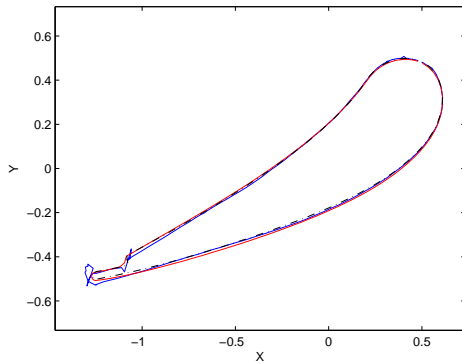
Figure 2-6: Dominant modes, trailing airfoil.



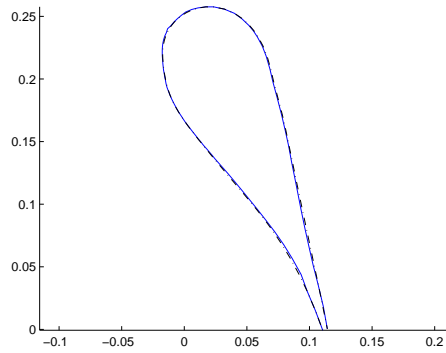
(a) Mode 3 on Type I



(b) Mode 3 on Type II



(c) Mode 4 on Type I



(d) Mode 4 on Type II

Figure 2-7: Dominant modes, trailing airfoil.

One can readily see differences between Type I and Type II in Figures 2-4 through 2-7. The first is in the shape of the trailing edge region: some of the dominant modes largely describe perturbation of the trailing edge and gill slot but as explained above, these modes cannot be fully expressed in the generated vanes. Another difference is that the deviations between the nominal geometry and each mode shape appear less substantial on the Type II vane. They are in fact of the same magnitude on each vane, and only look smaller because the Type II design is significantly larger than the

Type I. The distinctions between the dominant modes illustrated in Figures 2-4 and 2-5 and those in Figures 2-6 and 2-7 underscore the fact that the manufacturing of each airfoil is distinct, as mentioned in Section 2.2.1.

2.3 Vane Generation

The main purpose of decomposing the observed geometric variability into PCA modes is to enable the generation of a new vane population, as described in this section. Normally, this is done in order to create an experimental population for Monte Carlo analysis that is much larger than that which was measured. In this instance, a more important benefit is producing a perturbed set of vanes with a different design (Type II) than those measured (Type I), but which will employ the same manufacturing process. In this way, an engine manufacturer can acquire data to inform decisions on design and process improvements for a new engine before production begins. For this analysis, a total of 100 blades have been generated, 50 for each airfoil in the doublet.

A new, perturbed blade is formed by adding a weighted sum of the PCA modes to a baseline shape. Each mode is scaled by the product of the standard deviation of its amplitude σ with a Gaussian random value r (normally-distributed with zero mean and unit standard deviation). The latter brings about variation among the generated blades, while the former corresponds to a mode's scatter fraction and therefore ensures that the dominant modes occur with the same variability as in the original data set. The equation for the k^{th} point of the j^{th} generated vane is given by the following:

$$(x_{j,k}, y_{j,k}) = (x_k, y_k)_{\text{nominal, Type II}} + \sum_{i=1}^m (Cr_{i,j}\sigma_i(\hat{n}_k)_{\text{Type II}}\Delta n_{i,k})$$

$$C = \begin{cases} 0 & \text{in gill slot region} \\ 1 & \text{elsewhere} \end{cases} \quad (2.4)$$

$$\Delta n_{i,k} = (\hat{n}_k)_{\text{Type I}} \cdot (\Delta X_{i,k}, \Delta Y_{i,k})_{\text{Type I}} \quad (2.5)$$

The size and shape differences between the Type I and Type II vanes prevent one from directly applying the PCA modes derived from Type I to the Type II design. There is no direct correspondence between design geometry points from one design to the other, and in fact the Type II definition is comprised of fewer points than that for Type I. Therefore the Type I modes are mapped to the Type II vane based on fractional arc length, with each Type II point experiencing the mode amplitudes from the closest Type I point. The modes are initially defined in terms of x and y deviations from the mean, which only apply to the Type I vane. They are therefore expressed as normal deviations according to Equation 2.5 in which \hat{n}_k is the surface normal vector at the k_{th} node. As an operational design, the Type I definition includes a cooling gill slot near its trailing edge, which is a significant source of geometric variability. The more preliminary Type II definition lacks this feature, and so attempting to apply Type I's PCA modes to the Type II trailing edge will result in distorted, non-physical geometry. For this reason, there is simply no perturbation applied near the trailing edge of the Type II vane, as enforced by the variable C in Equation 2.4. Note that usually, the baseline to which the modes are applied is the average measured blade. In this case, there can be no average blade because the Type II design has not yet been put into production; therefore the nominal design is used instead. Although this does not take any average geometry perturbations into account, it is expected that such perturbations would not be substantial (and indeed the engine industry professionals consulted during this research have expressed confidence that the average blade and the nominal blade would be quite close in most respects[14]). Additionally, an average perturbation would affect all blades equally, and this research is more concerned with the distribution of the experimental population's performance and the causes thereof, rather than with the absolute performance values.

Chapter 3

CFD Analysis

3.1 Performance Scatter of Generated Vanes

3.1.1 Methods

The performance of the perturbed blade shapes is analyzed using the coupled Euler-boundary layer method MISES, developed by Drela and Youngren[9]. The boundary conditions consist essentially of a specified inlet angle and $\frac{P_{exit}}{P_{o,inlet}}$ ratio. The Reynolds number, based on axial chord, is approximately 770000; Sutherland's formula is used to determine the viscosity[1].

The Type II nominal design includes a round trailing edge, which MISES cannot currently accept[9], and which is therefore removed from the input. MISES instead utilizes a blunt trailing edge model. Recall from Section 2.3 that no perturbations could be applied to the trailing edge using PCA, so the omission of those points is of little consequence in and of itself. It must also be noted that the performance scatter calculations use non-planar geometry in that the streamtube radius as measured from the engine centerline and width are not constant.

Performance comparisons between vanes are made based on the following key quantities:

- Exit Mach number, M_2
- Exit/turning angle, α_2
- Inlet Mach number, M_1 , or flow rate
- Loss coefficient, $\bar{\omega}$, or total pressure loss, $\frac{\Delta p_o}{p_{o1}}$

The flow rate is only a function of the inlet Mach number because the inlet angle and the stagnation temperature and pressure are all fixed. The flow solver outputs the above critical quantities directly, with one exception: MISES calculates and outputs $\bar{\omega}$ according to the definition for compressors, as given below[9].

$$\bar{\omega}_{comp} = \frac{p_{o2}^{isen} - p_{o2}}{p_{o1} - p_1} = \frac{p_{o1} - p_{o2}}{p_{o1} - p_1} \quad (3.1)$$

The proper definition for a turbine is the following[16]:

$$\bar{\omega} = \frac{p_{o1} - p_{o2}}{p_{o2} - p_2} \quad (3.2)$$

During postprocessing, $\bar{\omega}$ is calculated from the MISES output using the equation below.

$$\bar{\omega} = \frac{1 - \frac{p_{o2}}{p_{o1}}}{\frac{p_{o2}}{p_{o1}} - \frac{p_2}{p_{o1}}} \quad (3.3)$$

Alternatively, one can directly convert the compressor loss coefficient that MISES outputs into the appropriate turbine definition using the following:

$$\bar{\omega} = \bar{\omega}_{comp} \frac{1 - \frac{p_1}{p_{o1}}}{\frac{p_{o2}}{p_{o1}} - \frac{p_2}{p_{o1}}} \quad (3.4)$$

Ideally, Equations 3.3 and 3.4 should give the same answer, but in actuality that is not the case due to the differences in the way the pressure ratios and $\bar{\omega}_{comp}$ are calculated. Except when otherwise noted, Equation 3.3 is used to calculate the loss coefficient, but Equation 3.4 is useful for finding the approximate relative contributions of viscous and inviscid losses. MISES outputs estimates for these using Equations 3.5

and 3.6[9], and the use of Equation 3.4 allows one to reframe them in turbine-specific terms. Note that in Equation 3.6, b is the streamtube thickness.

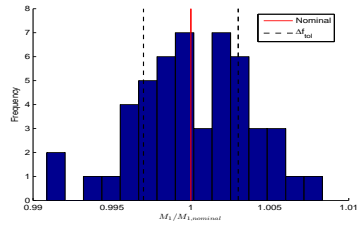
$$\omega_i = \frac{1}{p_{o1} - p_1} \int (p_o^{isen} - p_o) \frac{d\dot{m}}{\dot{m}} \quad (3.5)$$

$$\omega_v = \frac{1}{p_{o1} - p_1} \left(\frac{p_o}{p} \frac{\rho V}{\dot{m}} \rho V^2 \Theta b \right)_{exit} \quad (3.6)$$

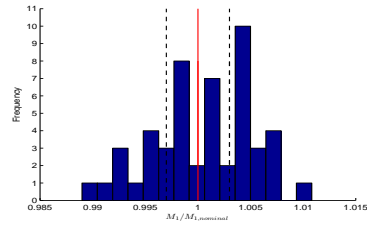
In a supersonic exit turbine like the one in this analysis, the above equations do not give exactly accurate answers because the momentum defect Θ does not asymptote to a constant downstream of the vane[9]. However, the relative contributions can still be assessed, if somewhat roughly.

3.1.2 Results

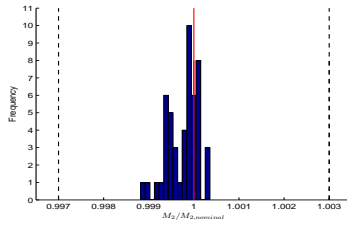
The distributions of the key performance quantities, as calculated by MISES, are shown in the following histograms. Since these results involve proprietary information, all quantities are scaled by their respective nominal value, except for the turning angle in which the nominal value is subtracted from each data point. The black dashed lines represent the acceptable range Δf_{tol} for each quantity: $\pm 0.3^\circ$ for turning angle, $\pm 0.3\%$ for inlet and exit Mach numbers, and $\pm 5\%$ for loss coefficient.



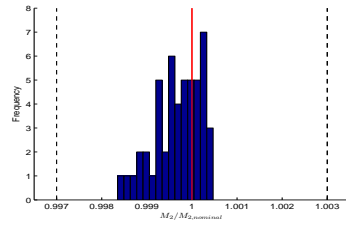
(a) Inlet Mach number,
leading airfoil



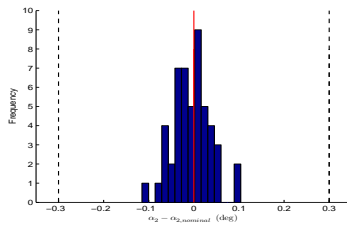
(b) Inlet Mach number,
trailing airfoil



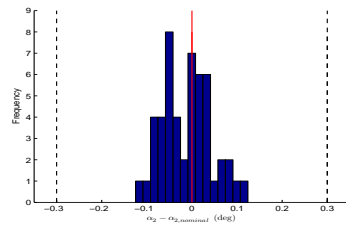
(c) Exit Mach number,
leading airfoil



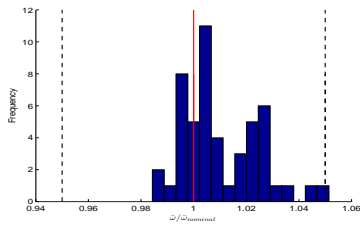
(d) Exit Mach number,
trailing airfoil



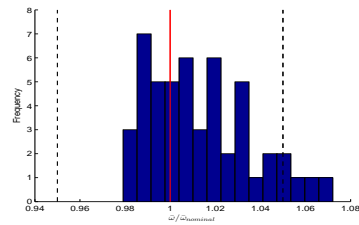
(e) Turning angle, leading
airfoil



(f) Turning angle, trailing
airfoil



(g) Loss coefficient, leading
airfoil

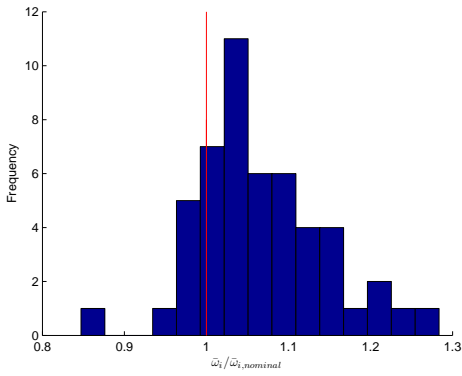


(h) Loss coefficient, trailing
airfoil

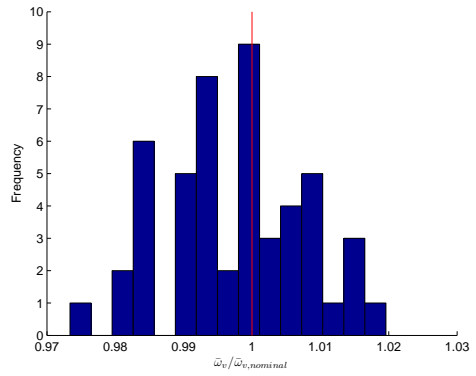
Figure 3-1: Distributions of performance quantities.

All vanes are well within the limits for exit Mach number and turning angle. With regards to losses, the leading airfoil performs unacceptably 2% of the time, while the trailing airfoil has approximately an 8% chance of non-conformance. The inlet Mach number is out of limits much more often: 36% of leading airfoils and 58% of trailing airfoils are more than 0.3% from the nominal. Some quantities are seen to have a centered distribution about the nominal value, whereas others (that have a high degree of dependence on shock mechanisms) are offset somewhat. For example, the offset-distributed exit Mach number is significantly influenced by shock behavior, whereas the centrally-distributed turning angle is much less so.

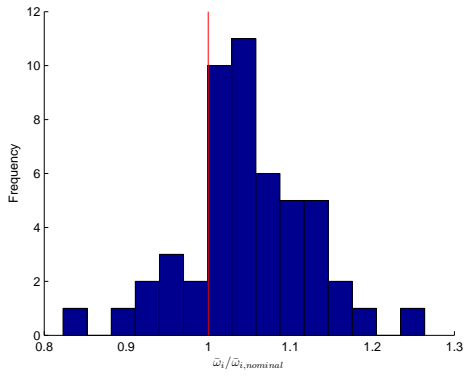
The viscous loss (Equation 3.6) and inviscid shock-loss coefficients (Equation 3.5) are distributed rather differently in the generated vane population, as illustrated in Figure 3-2. The viscous losses are approximately constant, varying by up to 3% of the nominal value, while the shock losses can be up to 30% than the nominal. This indicates that the increased total pressure loss in the generated vanes (i.e., the offset distribution) is likely due to shock effects rather than changes in boundary layer behavior.



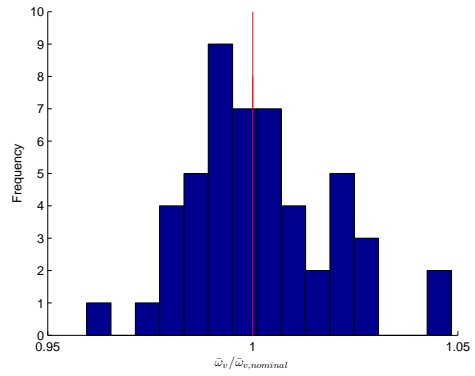
(a) Shock losses, leading airfoil



(b) Viscous losses, leading airfoil



(c) Shock losses, trailing airfoil



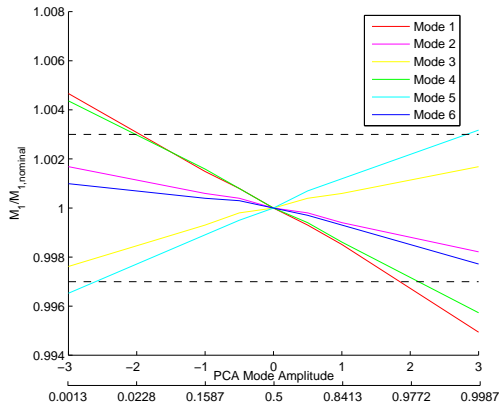
(d) Viscous losses, trailing airfoil

Figure 3-2: Inviscid and viscous loss coefficients of the generated vane population.

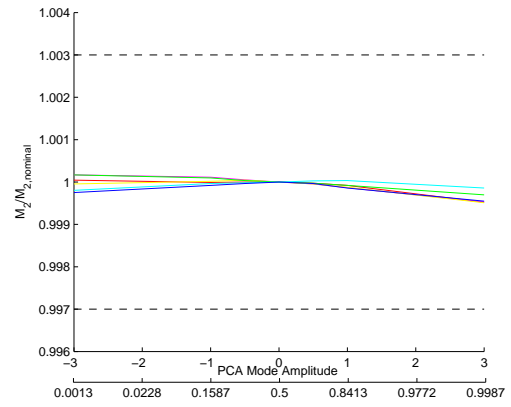
3.2 Sensitivity to PCA Modes

The PCA modes describe the expected variability of manufactured vanes, so it is useful to examine how individual modes affect performance. This is done by creating a series of vanes in which individual modes are expressed to varying degrees. The vane generation process is analogous to that described in Section 2.3, except that only one mode is applied at a time and the random scaling factor is replaced by a series of factors, in this case ± 3 , ± 1 , and ± 0.5 . Since the modes are still scaled by their respective scatter fractions, the end result is the application of modes with amplitudes of $\pm 3\sigma$, $\pm\sigma$, and $\pm 0.5\sigma$. The sensitivity is evaluated by examining each performance metric as a function of mode amplitude. The same non-planar geometry that is used as a baseline in the performance scatter estimate is used here as well, since the PCA modes are derived from measurements of the non-planar section.

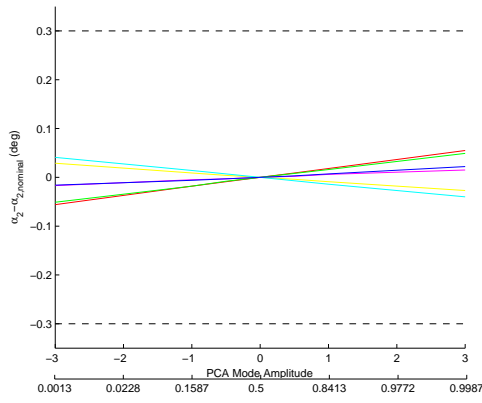
The effect of each airfoil's six most dominant PCA modes on the performance quantities is displayed in Figures 3-3 and 3-4. As in Figure 3-13, the dashed black lines represent the limits of acceptable performance. The second set of x-axis tick marks displays the cumulative distribution function values corresponding to each amplitude. These are based on the standard normal distribution[27] to which the PCA mode amplitudes conform (see Section 2.2.2).



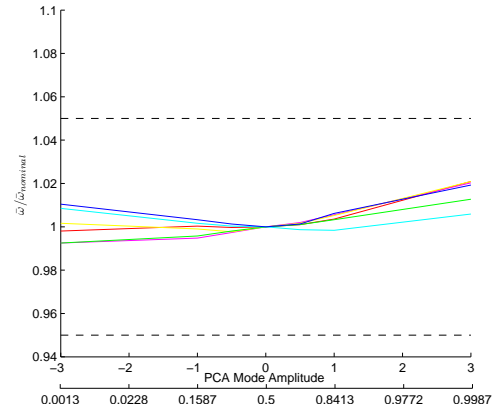
(a) Sensitivity of M_1



(b) Sensitivity of M_2

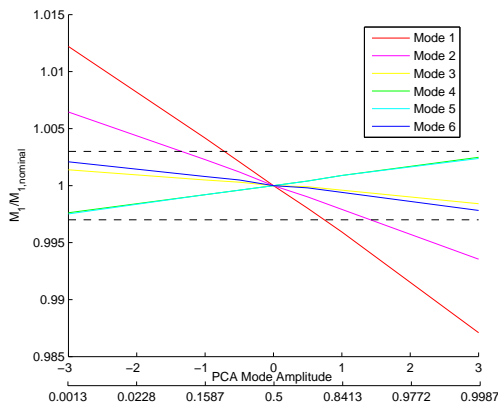


(c) Sensitivity of exit angle

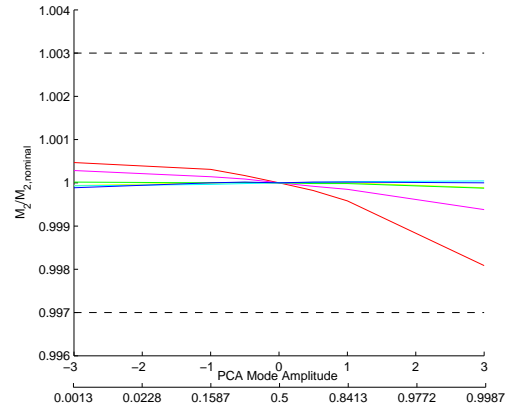


(d) Sensitivity of loss coefficient

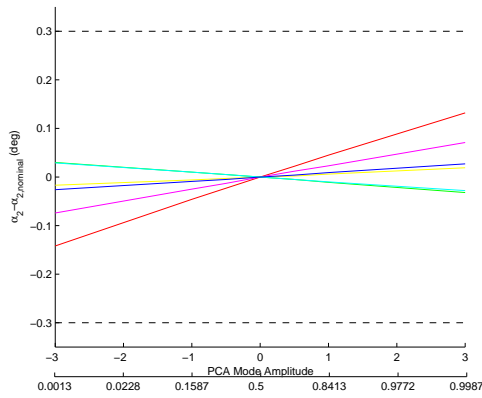
Figure 3-3: Sensitivity to dominant PCA modes, leading airfoil.



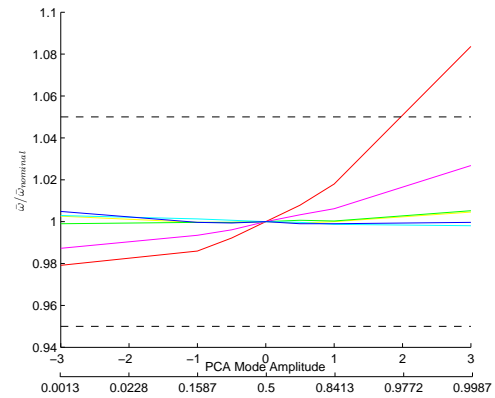
(a) Sensitivity of M_1



(b) Sensitivity of M_2



(c) Sensitivity of exit angle



(d) Sensitivity of loss coefficient

Figure 3-4: Sensitivity to dominant PCA modes, trailing airfoil.

As expected, the modes with the highest scatter fraction generally have more of an effect on the flow. The leading airfoil's fourth mode appears to have a greater influence on the inlet Mach number than anticipated because it has an unusually large outward deviation near the throat, as shown in Figure 2-5 (Section 3.3.1 shows that the inlet Mach number depends most strongly on the throat geometry). The inlet Mach number has a nearly linear response to the amplitude of each mode since the throat area scales with mode amplitude in simple linear fashion. According to these

results, a single dominant PCA mode can cause inlet Mach number nonconformance at above the approximate $\pm 2\sigma$ level for the leading airfoil and the $\pm\sigma$ level for the trailing. Based on the standard normal distribution to which the mode amplitudes conform, the probabilities that an individual mode will be expressed at that level are roughly 5% and 32%, respectively.

Nonlinearity is evident in the sensitivity of the loss coefficient and to a lesser extent the exit Mach number. Nonetheless, there is only one excursion outside the acceptable performance range for these parameters; in every other case the chance that a single mode will cause unacceptable performance is less than 0.26%. The probability is the same for the more linear turning angle. The trailing airfoil's first mode is seen to bring about unacceptably high losses at around the $+2\sigma$ level, and the probability of this occurring is about 2.5%. Loss coefficient nonconformances happen at a slightly higher rate in Figure 3-1, likely due to additive effects from the other modes, particularly mode 2.

3.3 Sensitivity to Localized Bump Perturbations

The next main segment of this work is the use of linear and nonlinear sensitivity analysis to identify locations on the vane surface where geometric perturbations have the greatest effect on performance.

3.3.1 Linear Sensitivity in MISES

Methods

This analysis makes use of MISES' functionality to calculate linear sensitivity derivatives with respect to the amplitudes of a series of geometry perturbation modes, which are used to virtually move the airfoil surface.

The flow analysis performed in this section is different from that described in Sections 3.1 and 3.2. Specifically, to enable comparison with the discontinuous-Galerkin method in Chapter 4, the analysis is planar (i.e., no radius variation) and the stream-tube thickness is constant.

This section contains analysis of the sensitivity to localized small bumps. The purpose is to determine where geometry perturbations are most/least detrimental to performance. This analysis, due to its linearity, could also be used to consider linear sensitivity of other perturbations using a linear combination of the localized bump sensitivities. This has not been pursued in this thesis, but remains an opportunity for future work.

The specific bump shape is the Hicks-Henne function[15], which is commonly used to perturb airfoil surfaces[5][17]. Its definition is given in Equation 3.7[26].

$$y = A \left[\sin \left(\pi x \frac{-\ln 2}{\ln x_p} \right) \right]^t, x \in [0, 1] \quad (3.7)$$

In the above equation, y corresponds to the normal displacement and x is the distance along the airfoil surface, A represents the amplitude, x_p is the location of the maximum, and t defines the sharpness of the bump. For this work, A is simply set to 1, x_p is 0.5

to produce a centered bump, and t is 5, reducing Equation 3.7 to $y = \sin^5 \pi x$. Below is a plot of that function.

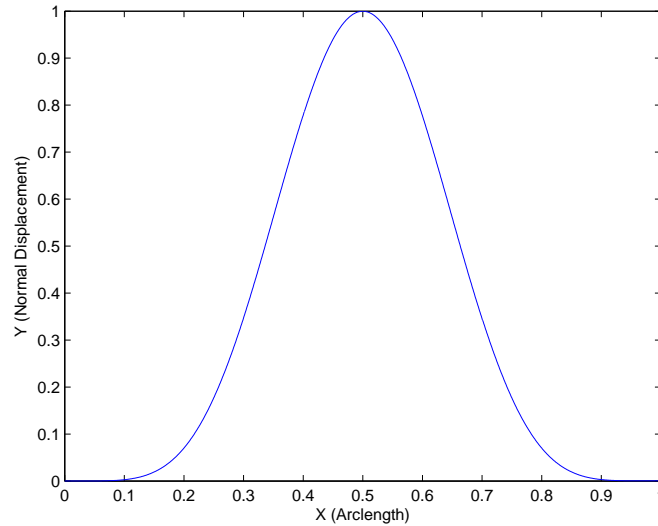


Figure 3-5: Hicks-Henne bump function used to perturb airfoil geometry.

Almost all modes are applied between surface definition points $i - 1$ and $i + 1$, with the midpoint approximately corresponding to point i , meaning that the mode is essentially a smoothed normal perturbation of that point. The only exceptions are the first and last modes which must lie between the first two and last two points, respectively. The modes are thus distributed so that, taken together, they span the entire airfoil surface. MISES uses each mode shape to apply a virtual perturbation to the airfoil surface and then calculates the linear sensitivity derivative with respect to mode amplitude for key performance quantities like Mach number, static pressure over inlet total pressure, loss coefficient $\bar{\omega}$, and flow slope S , which is equal to the tangent of the flow angle α . The latter is again calculated in MISES according to Equation

3.1 and is converted to the turbine definition of Equation 3.2 as follows:

$$\begin{aligned} \frac{d\bar{\omega}}{d[Mode]} = & \frac{d\bar{\omega}_{comp}}{d[Mode]} \frac{1 - \frac{p_1}{p_{o1}}}{\frac{p_{o2}}{p_{o1}} - \frac{p_2}{p_{o1}}} - \frac{\bar{\omega}_{comp}}{\frac{p_{o2}}{p_{o1}} - \frac{p_2}{p_{o1}}} \frac{d\left(\frac{p_1}{p_{o1}}\right)}{d[Mode]} + \\ & + \bar{\omega}_{comp} \frac{1 - \frac{p_1}{p_{o1}}}{\left(\frac{p_{o2}}{p_{o1}} - \frac{p_2}{p_{o1}}\right)^2} \frac{d\left(\frac{p_2}{p_{o1}}\right)}{d[Mode]} - \bar{\omega}_{comp} \frac{1 - \frac{p_1}{p_{o1}}}{\left(\frac{p_{o2}}{p_{o1}} - \frac{p_2}{p_{o1}}\right)^2} \frac{d\left(\frac{p_{o2}}{p_{o1}}\right)}{d[Mode]} \end{aligned} \quad (3.8)$$

It is the exit or turning angle α_2 rather than the exit slope S_2 that is of interest, so the sensitivity derivative of the former is found using Equation 3.9, given below. The negative sign is necessary because the exit slope is negative on the axes used in this analysis but, according to convention, the turning angle is to be quoted as a positive value.

$$\frac{d\alpha_2}{d[Mode]} = -\frac{dS_2}{d[Mode]} \cos^2 \alpha_2 \quad (3.9)$$

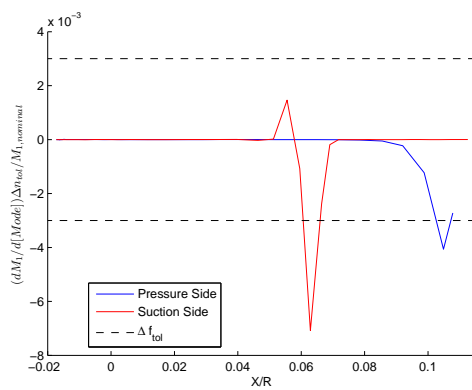
Often, manufacturing tolerances include a maximum allowable surface deviation, Δn_{tol} that is defined as the maximum allowable normal perturbation from the design intent shape. Thus, Δn_{tol} defines a band of allowable shapes surrounding the design intent. In the following linear sensitivity analysis, Δn_{tol} is used to determine the performance perturbation that would result from a bump of height Δn_{tol} . For each performance metric f , the performance deviation for the turning angle is $\frac{df}{d[Mode]} \Delta n_{tol}$. Tolerances are also placed on the performance quantities, i.e., there is a maximum allowable Δf_{tol} (see Section 3.1.2). One can compare that value to the linear sensitivity estimate to determine if a perturbation will cause unacceptable performance.

The linear sensitivity derivatives are calculated for both viscous and inviscid flow. For the inviscid runs to be successful, the Type II vane geometry must be modified so that the trailing edge is cusped. Recall from Section 3.1 that the nominal geometry includes a rounded trailing edge, which must be left out of the shape that is input into MISES, and that a blunt trailing edge model is utilized in its place. The use of this model causes difficulties in an inviscid calculation: MISES assumes that a constant-thickness streamtube exists on the blunt trailing edge in an inviscid flow[8].

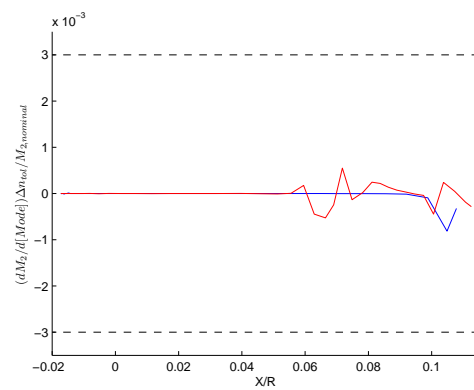
To improve the physical modeling, a more realistic approach is to cusp the trailing edge so that the trailing edge streamtube has zero thickness.

Viscous Results

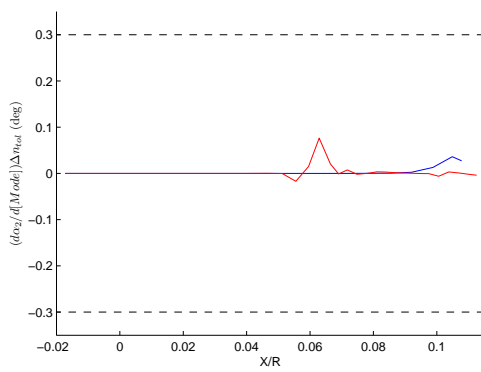
The viscous linear sensitivity with respect to bump mode amplitude is shown in Figure 3-6. Note that all results are scaled by the nominal value, except in the case of the turning angle.



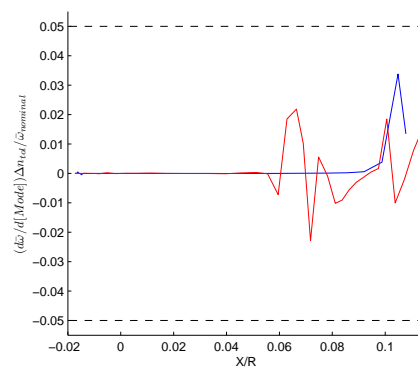
(a) Sensitivity of M_1



(b) Sensitivity of M_2



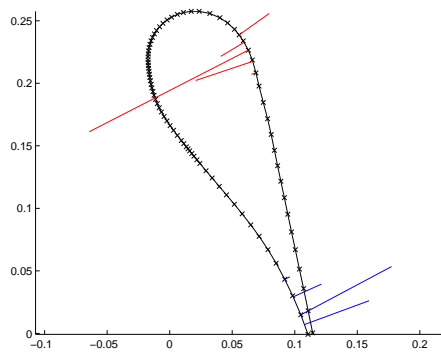
(c) Sensitivity of exit angle ($^{\circ}$)



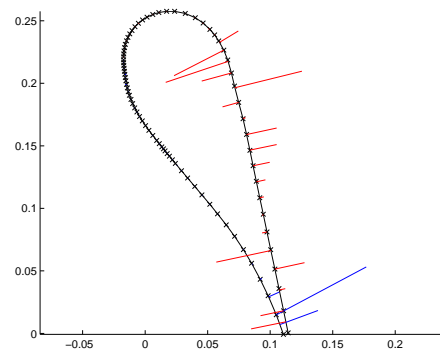
(d) Sensitivity of loss coefficient

Figure 3-6: Linear sensitivity results from viscous MISES calculations.

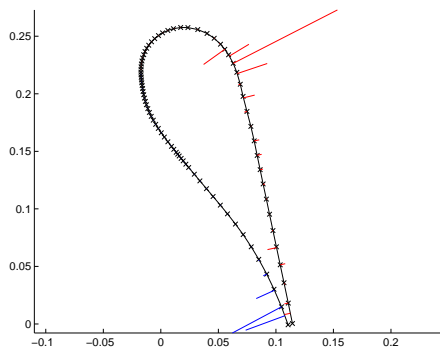
Figure 3-6 shows that the sensitivity is restricted to less than half of the vane's surface, outside of which the derivatives are insignificant. In order to more clearly illustrate the locations of high sensitivity, Figure 3-7 represents each derivative by the length of a surface normal vector located at the midpoint of the associated bump mode. An outward-pointing vector indicates a positive derivative, meaning that an outward displacement will cause the quantity in question to increase. Note that Figure 3-7 follows the same color convention as Figure 3-6 in that the vectors representing pressure-side derivatives are blue and those corresponding to the suction-side are red.



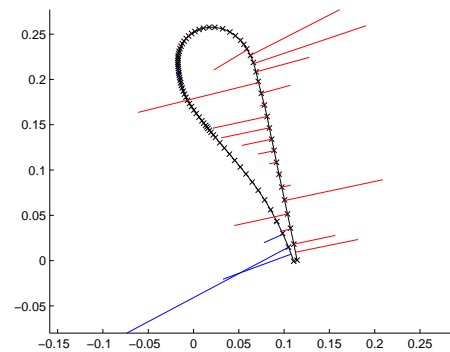
(a) Sensitivity of M_1



(b) Sensitivity of M_2



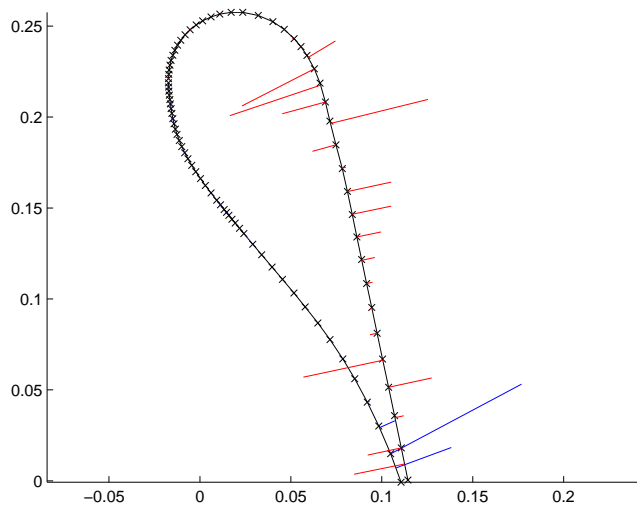
(c) Sensitivity of exit angle



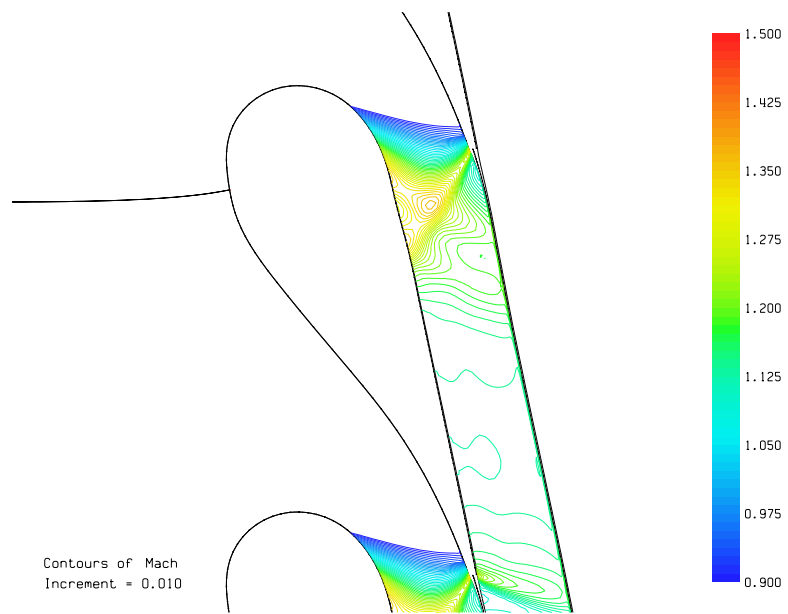
(d) Sensitivity of loss coefficient

Figure 3-7: Normal-vector representation of viscous MISES linear sensitivity derivatives.

Figure 3-8 illustrates that the sensitivity derivatives begin to take on significant values only once the flow reaches sonic speed at the throat; the region of near-zero sensitivity is upstream of the throat. Geometry perturbations in the supersonic flow region are likely to cause shocks which will cumulatively cause significant changes to the flow, hence the nonzero sensitivity derivatives. A geometry change near the location of an existing shock is likely to change the shock's strength and/or cause it to occur at a different location, either of which will have a marked effect on the flow field. Perturbing the airfoil surface near the throat itself will cause the throat to widen or narrow, changing the mass flow through the passage which affects the Mach number and consequently the shock losses. The throat is located very near to the suction side inflection point, and its high sensitivity is thus reinforced by the work of Denton and Xu who show that loss is particularly sensitive to blade suction side curvature[7]. There is further support for the fundamental validity of these data in the well-established fact that loss generation is much higher on the suction side of a blade (where most of the sensitivity lies) than on the pressure side (which is largely insensitive)[20]. This result holds for subsonic as well as transonic blades because entropy generation is proportional to the cube of surface velocity. The suction side/pressure side disparity in loss generation will be amplified in a transonic blade because shocks can be present in the supersonic flow over the suction side but cannot occur on the vast majority of the pressure side.



(a) Sensitivity of M_2



(b) Mach contours

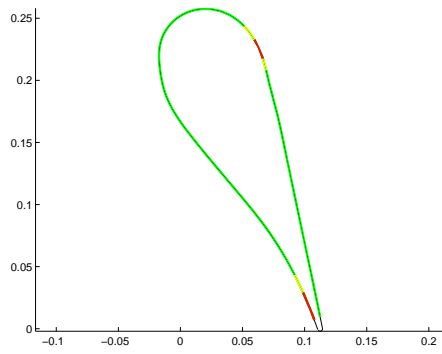
Figure 3-8: Sensitivity derivatives compared with Mach contours.

The notion that the sensitivity derivatives are associated with shock behavior is supported by results from the performance scatter estimate of Section 3.1, specifically the distributions of viscous and inviscid loss coefficients as shown in Figure 3-2. If geometric differences between blades express themselves more prominently through inviscid mechanisms, then it stands to reason that geometry perturbations in the supersonic flow region will have a much greater effect on the flow field than those in the subsonic regime, and that perturbations near the throat or existing, comparatively strong shocks will have the greatest effect of all.

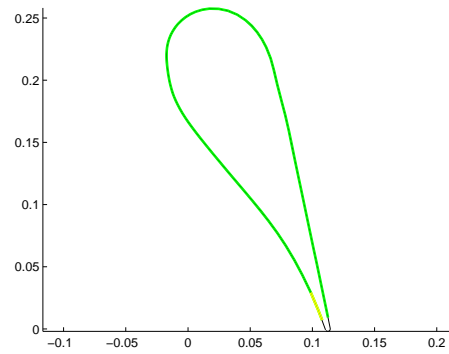
If the performance scatter results can help inform and confirm the sensitivity behavior, then the converse can be done as well. For an optimized vane such as this one, perturbations in the supersonic flow region are expected to decrease performance, primarily through the generation or modification of shocks. That is, over much of the sensitive region, any changes can only make things worse. However, opening the throat will increase the inlet and exit Mach numbers by continuity and closing it will have the opposite effect, so perturbations near the throat could in fact “improve” Mach numbers (in practice, one wants the vane to produce an exit Mach number that is as close as possible to the nominal value to which the rotor stage is optimized- a higher inlet Mach number to the rotor will decrease its efficiency). The distribution of inlet Mach number is thus centered because it is essentially dependent on throat area alone, and the distributions of losses and exit Mach number are offset from the nominal because they are additionally subject to the worsening effects of shock generation. The linear sensitivity results also highlight a limitation of the performance scatter estimate. Recall that the trailing edge is not perturbed at all among the generated vanes. Since the linear sensitivity analysis indicates that the trailing edge is one of the most sensitive regions of all, the results of Section 3.1.2 almost certainly underestimate the scatter.

For the designer and manufacturer, the practical value of these results lies chiefly in their use as a guide for setting or adjusting tolerances. The preceding identifies the highly-sensitive “hotspots” on the vane; it is worthwhile to find out just how hot they are from a manufacturing standpoint by converting the sensitivity derivatives

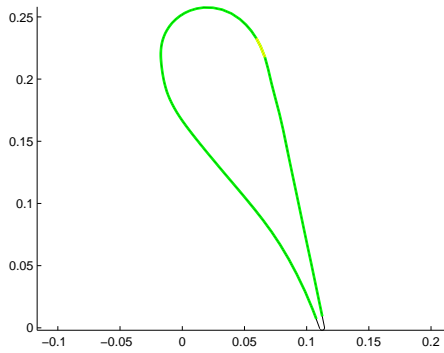
into geometric tolerances. These are calculated by multiplying the reciprocal of the derivative by Δf_{tol} . The resulting shape envelopes are compared to the nominal tolerance on local deviations Δn_{tol} in Figure 3-9. Red sections of the envelope are those in which Δn_{tol} allows a greater performance deviation than specified, meaning that it needs to be tightened. In yellow sections, the derivatives are nonzero but Δn_{tol} is enforced (and plotted) because it is tighter than that stipulated by the derivatives. The nominal tolerance is plotted in green sections as well, but these correspond to areas where near-zero sensitivity derivatives indicate that Δn_{tol} can be widened by a factor of 5 or more. Note that the envelopes are formed based on single-point deviations, that is, if one point in a red zone is outside of the envelope, the vane's performance will be out of the limits.



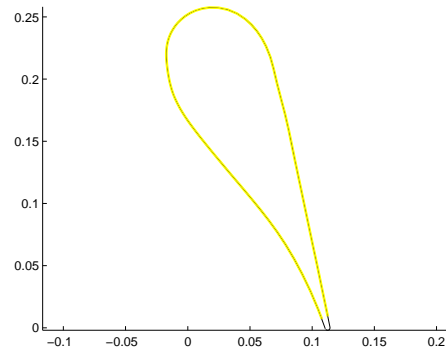
(a) 0.3% change in M_1



(b) 0.3% change in M_2



(c) 0.3° change in α_2



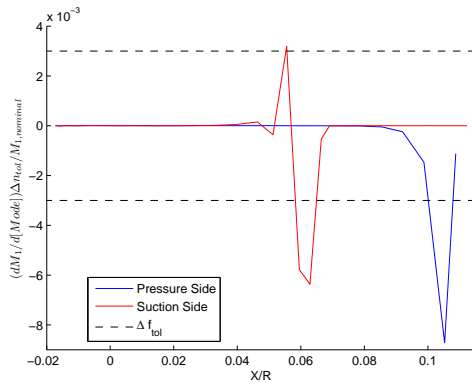
(d) 5% change in loss coefficient

Figure 3-9: Tolerance bands for specified performance limits.

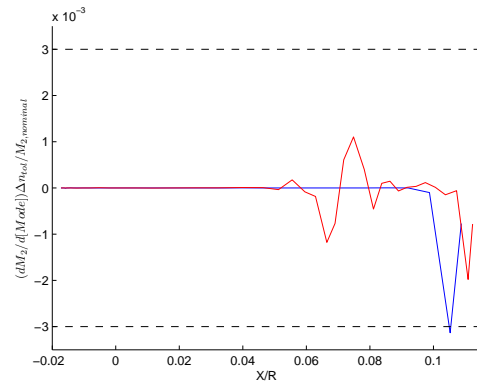
Over much of the vane, Δn_{tol} is sufficient to keep the performance within the specified limits. Three of the performance metrics indicate that it can even be virtually abolished over most of the vane, but the 5% limit on the loss coefficient prohibits this. Only near the throat is the nominal tolerance inadequate, as perturbations within it can drive the inlet Mach number (flow rate) outside of the stipulated range.

Inviscid Results

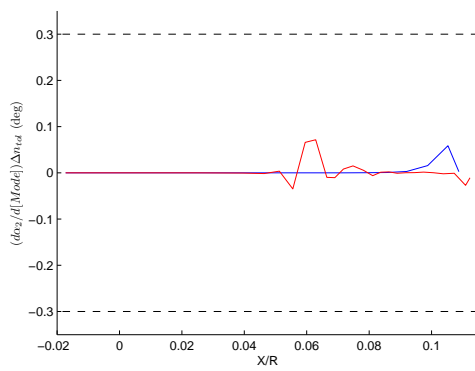
The linear sensitivity results for inviscid flow are shown in Figures 3-10 and 3-11.



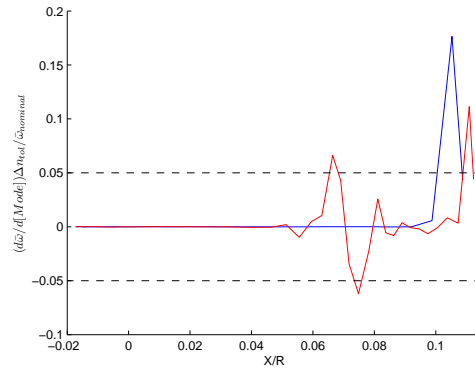
(a) Sensitivity of M_1



(b) Sensitivity of M_2

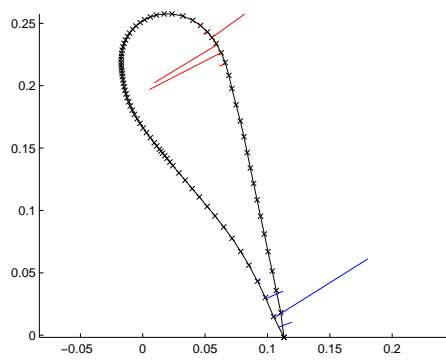


(c) Sensitivity of exit angle

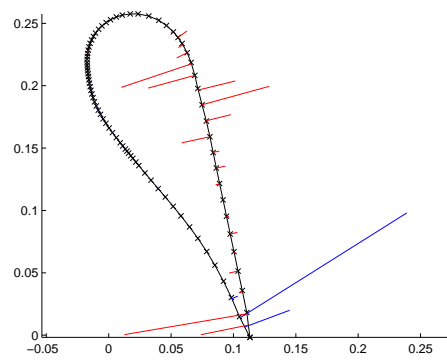


(d) Sensitivity of loss coefficient

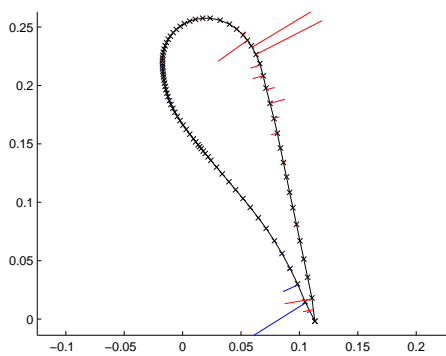
Figure 3-10: Linear sensitivity results from inviscid MISES calculations.



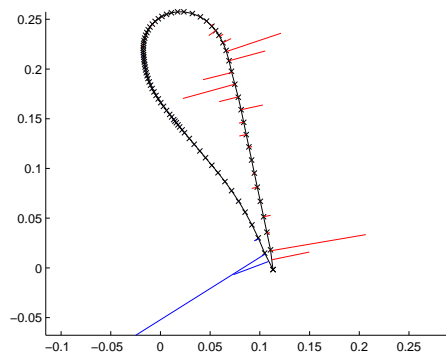
(a) Sensitivity of M_1



(b) Sensitivity of M_2



(c) Sensitivity of exit angle



(d) Sensitivity of loss coefficient

Figure 3-11: Normal-vector representation of inviscid MISES linear sensitivity derivatives.

The inviscid linear sensitivity derivatives largely follow the same trends as their viscous counterparts (see Figures 3-6 and 3-7), with one notable exception: the sign of the derivatives at the suction side trailing edge. The sign does not change in the inviscid results whereas it oscillates between positive and negative in the viscous results. The most likely cause of this discrepancy is the presence/absence of the blunt trailing edge model. The magnitudes of the derivatives are similar, with the inviscid

results generally exhibiting greater sensitivity than their viscous counterparts. Shock-boundary layer interaction[6] can act to damp out the effects of shocks near the surface of an airfoil by concealing small perturbations which could potentially generate shocks within the displacement thickness. Although individually weak, those shocks would have a cumulative effect that would likely increase losses to a significant degree. Since the boundary layer is absent from inviscid flow, it stands to reason that the linear sensitivity derivatives should be higher in an inviscid flow.

3.3.2 Nonlinear Sensitivity Analysis

Methods

Nonlinearity is explored in regions of the vane surface that are identified by the viscous linear sensitivity analysis as being particularly sensitive. The critical results of these runs are the performance quantities as functions of normal displacement. Individual geometry nodes are given a series of finite normal perturbations and the resulting set of vanes is analyzed in MISES using viscous calculations. In contrast to the MISES linear sensitivity analysis, these perturbations are real rather than virtual. However, moving one node a short distance in the normal direction is approximately equivalent to applying a bump mode of small amplitude since the midpoint of the i^{th} geometry perturbation mode is very close to the i^{th} point (see Section 3.3.1). This similarity allows for comparisons between the linear and nonlinear sensitivity behavior.

Results

Nonlinear sensitivity is evaluated at four especially sensitive locations: both sides of the throat (nodes 2 and 68), a point (node 72) in the supersonic flow region just after the throat, and the suction side trailing edge (node 84). Those points are displayed in Figure 3-12.

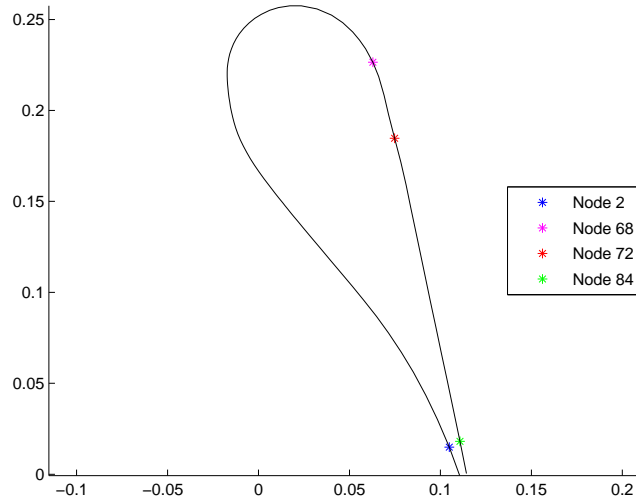
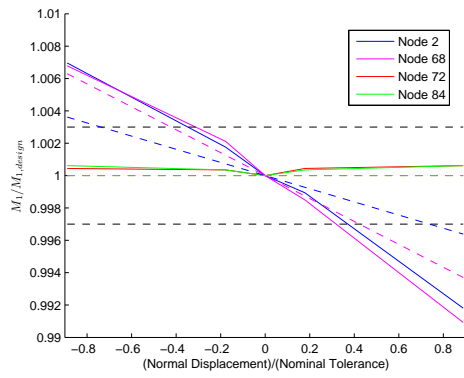
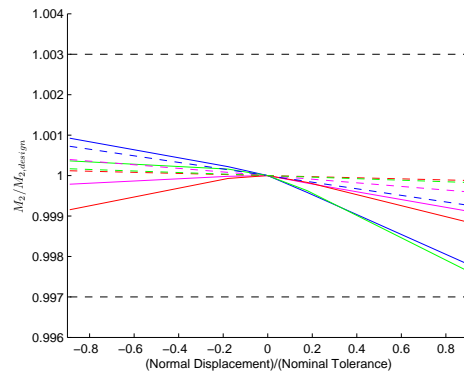


Figure 3-12: Locations at which nonlinear sensitivity is investigated.

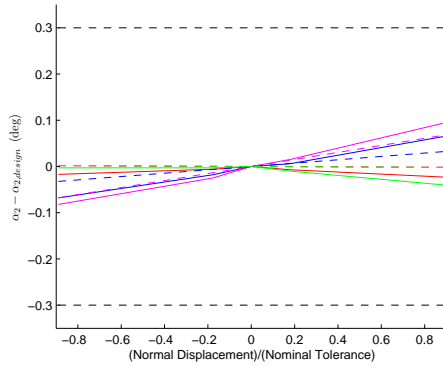
The nonlinear sensitivity of the performance metrics at these four nodes is shown in Figure 3-13. The dashed black lines display the performance limits Δf_{tol} , and the dashed colored lines are the linear sensitivity results. All quantities are nondimensionalized by their respective nominal values.



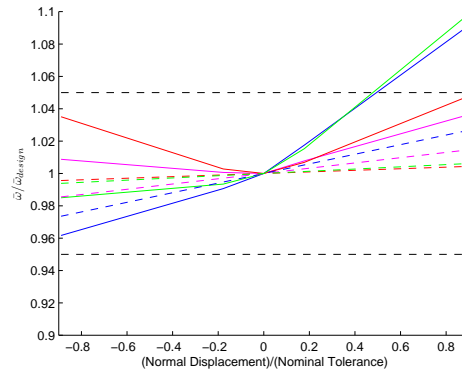
(a) Sensitivity of M_1



(b) Sensitivity of M_2



(c) Sensitivity of exit angle



(d) Sensitivity of loss coefficient

Figure 3-13: Nonlinear sensitivity results.

The sensitivity observed here is almost universally higher than that predicted by the linear analysis. Logically, there is closer agreement between linear and nonlinear results for smaller perturbations; nonlinearity makes more of a difference as the geometry is displaced farther from the nominal, particularly in the case of the loss coefficient. The nonlinearity in loss coefficient observed at nodes 68 and 72 on the suction side indicates that the airfoil shape is indeed optimal at these locations with regards to losses because perturbation in either direction causes losses to increase.

Since the maximum normal displacement applied here is slightly less than the nominal tolerance Δn_{tol} , these nonlinear results indicate that Δn_{tol} may in fact not be adequate to control losses at the trailing edge. The inlet Mach number shows more sensitivity than the exit Mach number according to both linear and nonlinear analysis, which is reasonable due to the basic geometry of the vane passage. Figure 3-8 illustrates that $\frac{A_2}{A^*}$ is not much greater than unity while $\frac{A_1}{A^*}$ is an order of magnitude larger, meaning that the latter will scale more dramatically with A^* . In sum, these results suggest that with the nominal tolerance in place, Type II vanes manufactured according to the same process as Type I should be entirely capable of producing a properly conditioned exit flow with regards to speed and direction. Losses may be unacceptably high, though, and the flow rate through a given passage is likely to be out of limits. The near-constant slope of the latter means that, barring any bias in the manufacturing process towards plus- or minus-material, there will likely be as many high-flowing passages as there are low-flowing ones so the total flow rate through the vane row should be acceptable. The results in Figure 3-1 bear this out, showing a centered distribution of inlet Mach number. Nevertheless, uniformity is desirable and for that reason particular attention must be paid to the throat area.

The nonlinear bump sensitivity of inlet Mach number is compared to both the isentropic relation between Mach number and area change[23] and data extracted from the PCA mode sensitivity analysis of Section 3.2 in Figure 3-14. For the latter, the throat area change is based on the perturbation of node 68; recall that, as part of the trailing edge, node 2 is not perturbed by the PCA modes in this analysis. Comparison shows that both data sets closely follow the isentropic trend, particularly for small perturbations. The isentropic relation supports the observation in Section 3.3.1 that Δn_{tol} (the vertical dashed black lines) is not sufficient to keep the inlet Mach number within $\pm\Delta M_{1,tol}$ (the horizontal dashed black lines).

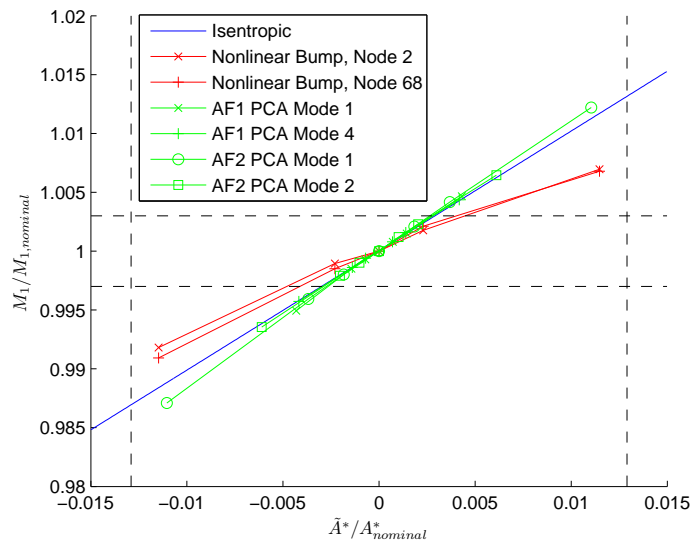


Figure 3-14: Comparison of inlet Mach number sensitivity.

Chapter 4

Comparison with Discontinuous-Galerkin Sensitivity Results

An alternative method of calculating linear sensitivity derivatives makes use of a discontinuous-Galerkin (DG) solver currently in development at the MIT Aerospace Computational Design Laboratory[4][11][10][22]. The objective of this segment of the research is to obtain independent confirmation of the sensitivity behavior observed in the MISES results.

4.1 Methods

The DG solver, known as ProjectX, does not yet have the capability to directly perform linear sensitivity calculations, so the derivatives are found using finite differencing. Also, presently its turbulence modeling has not been applied to turbomachinery[3][21] so all runs are inviscid.

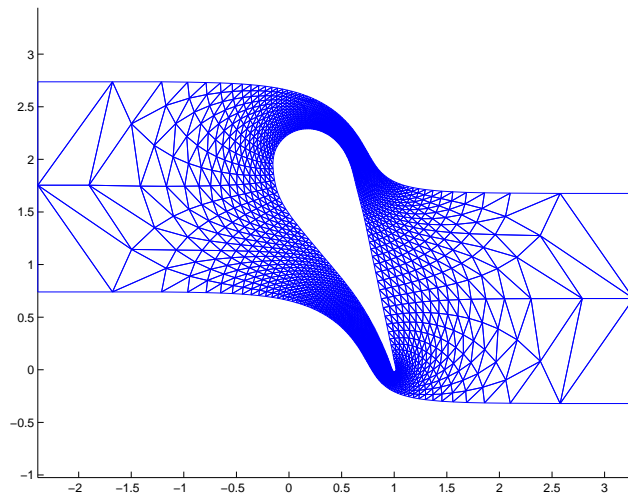
The following boundary conditions are utilized throughout the DG runs. The flow angle, total pressure and total temperature at the inlet along with the exit static pressure ratio are set to the same values used in MISES. The top and bottom boundaries

of the grid are designated as periodic, simulating a blade row, and flow tangency is enforced on the airfoil surface.

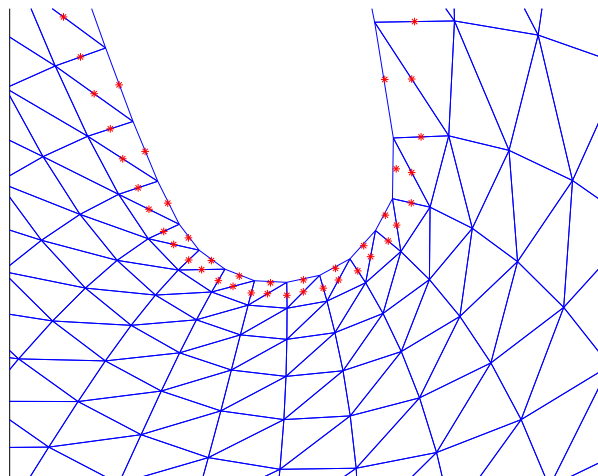
The baseline grid used in DG calculations is modified from one supplied by Rolls-Royce, with the following changes being made:

- Dividing each (4-sided) element into two triangular elements.
- Moving the nodes on the lower boundary face in the y direction so as to make the height of the grid constant along its length. Although the changes are very slight, this ensures that there will be no difficulties enforcing the periodic boundary condition at the upper and lower boundary faces.
- Representing the elements on the airfoil as quadratic polynomials (instead of the straight-line segments in the original mesh) by adding midpoint nodes to their faces[2]. The midpoint nodes on the airfoil surface are generated by splining the surface nodes from the original mesh. The other midpoint nodes are simply co-linear (i.e. the interior edges remain linear).

The nominal grid is shown in Figure 4-1, with the added nodes highlighted in red.



(a) Grid



(b) Quadratic elements

Figure 4-1: Nominal grid for DG cases.

The converged nominal case is the basis for each of the linear sensitivity runs via the substitution of a perturbed grid into the nominal solution file. The perturbed grids are intended to mimic as closely as possible the perturbations used in MISES. Hicks-Henne bump functions of finite amplitude are applied to the airfoil surface over the same fractional arc length limits as in MISES, so that the resulting sensitivity derivatives have a direct correspondence to those in Section 3.3.1. Note that the midpoint nodes of the interior edges are affected by the surface perturbation, as they are re-positioned to be at the midpoints of the new elements' faces. Two grids are generated for each arc length interval: one with positive bump function amplitude, and one with negative. The sensitivity derivative for a performance quantity f is found through finite differencing of the results from the positive- and negative-amplitude cases, according to the following equation:

$$\frac{df}{d(\Delta n)} = \frac{f^+ - f^-}{2(\textit{Amplitude})} \quad (4.1)$$

Like in MISES, bump function amplitude and maximum normal displacement are by definition the same.

4.2 Results

The finite-difference linear sensitivity derivatives are displayed in Figure 4-2.

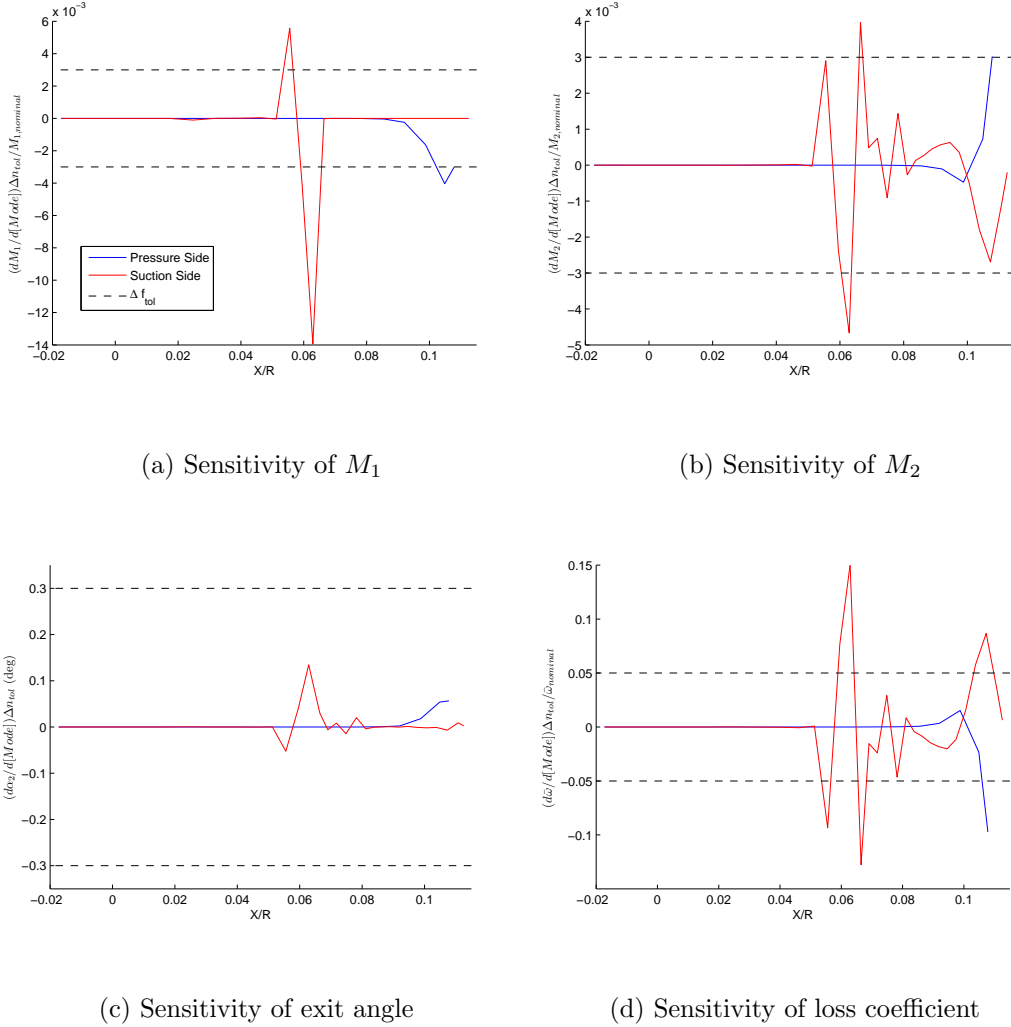
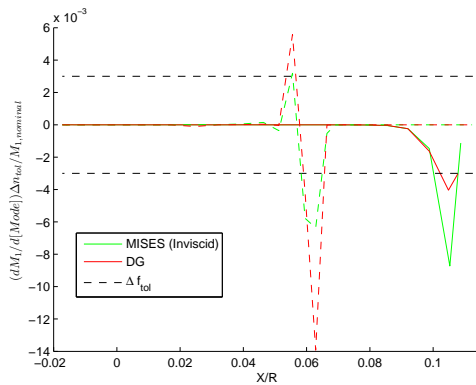


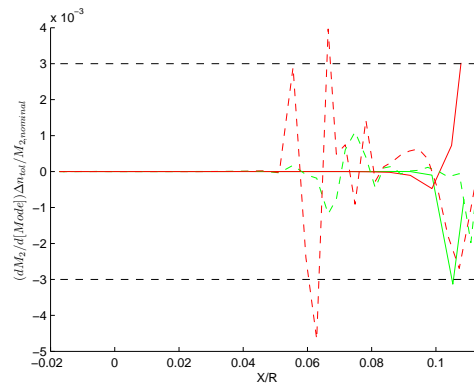
Figure 4-2: Linear sensitivity calculated via DG method.

Figure 4-2 show that the inviscid DG linear sensitivity derivatives largely follow the same trends as the viscous MISES results in Figure 3-6 , a further indicator that the sensitivity is primarily dependent on inviscid mechanisms. The trends deviate from each other on both sides of the trailing edge, which is possibly due to the workings of MISES' blunt trailing edge model. The model is not active in the inviscid MISES

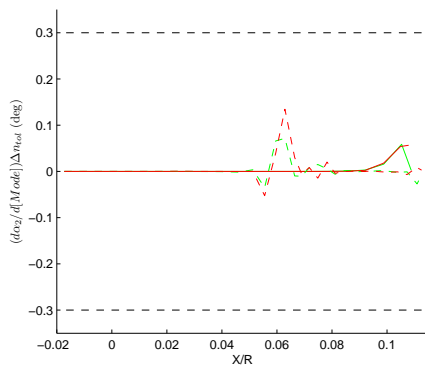
calculations, but the two sets of inviscid results still have opposite signs on the pressure side trailing edge for the exit Mach number and loss coefficient derivatives. Each solver uses a different geometry at the trailing edge, though, with a cusp in MISES and a round in DG. For ease of comparison, both sets of inviscid linear sensitivity data are plotted together in Figure 4-3. Note that solid lines correspond to the pressure side and dashed lines correspond to the suction side.



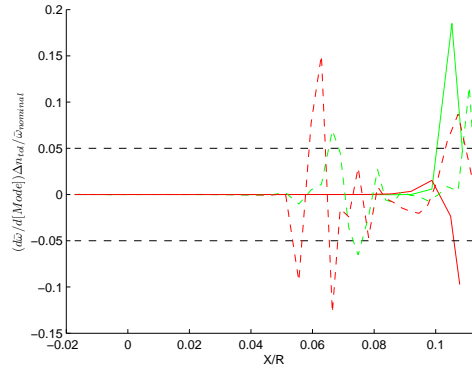
(a) Sensitivity of M_1



(b) Sensitivity of M_2



(c) Sensitivity of exit angle

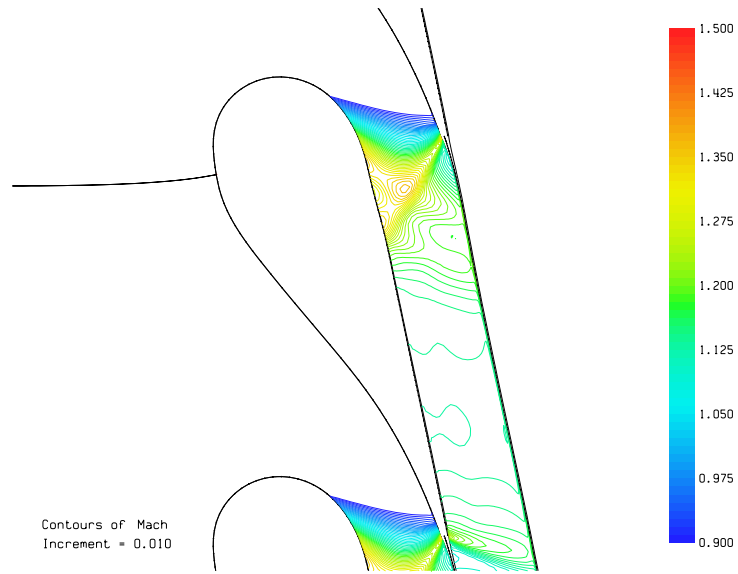


(d) Sensitivity of loss coefficient

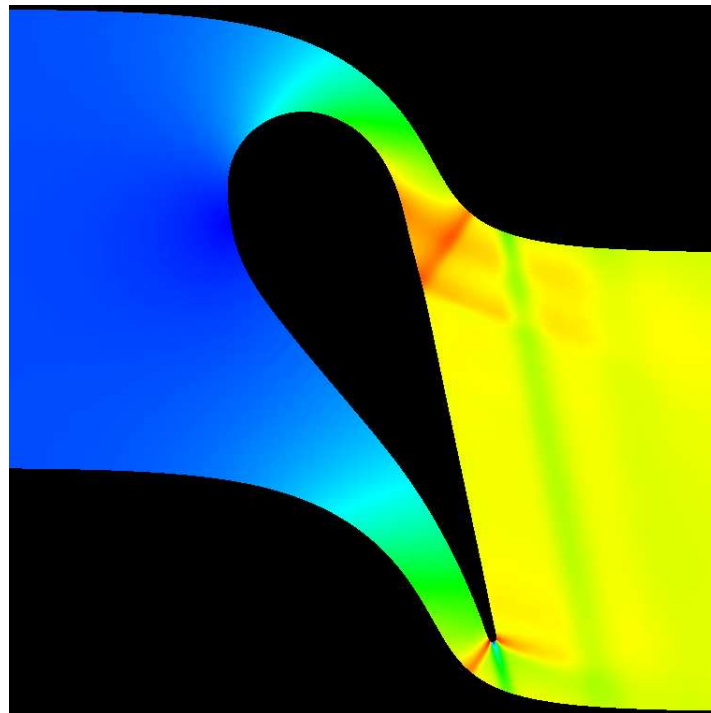
Figure 4-3: Comparison of linear sensitivity results.

The Mach contours from MISES and DG are shown in Figures 4-4 through 4-6 for

the nominal case and for perturbations near the throat (at nodes 2 and 68, the same as in Section 3.3.2). The most noticeable difference between the three cases is in the shock behavior on the suction side. When the node 68 perturbation is compared to the other two cases, its shock structure is seen to be somewhat more spread out along the surface. In MISES, the nominal structure appears only to be stretched, whereas the formation of a new weak shock is observed in the DG results. This may be the source of the greater sensitivity seen in DG. Once ProjectX is developed further, future work could investigate whether or not the sensitivity remains higher when viscous effects are included.

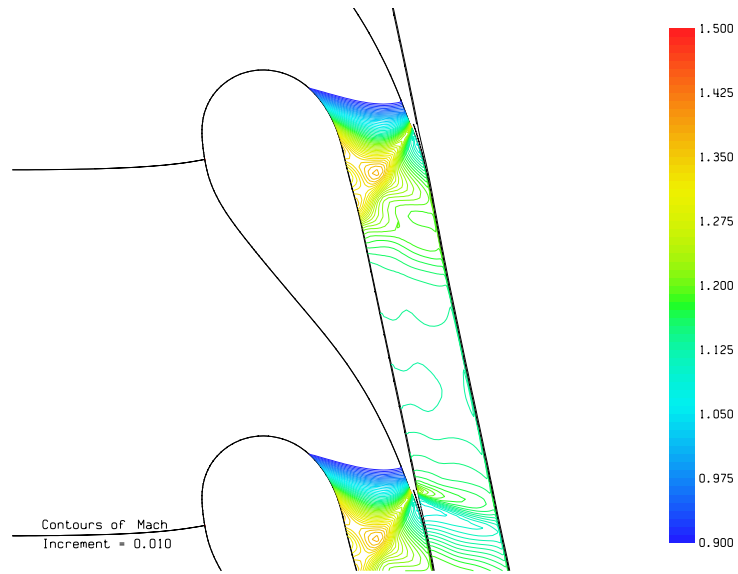


(a) MISES

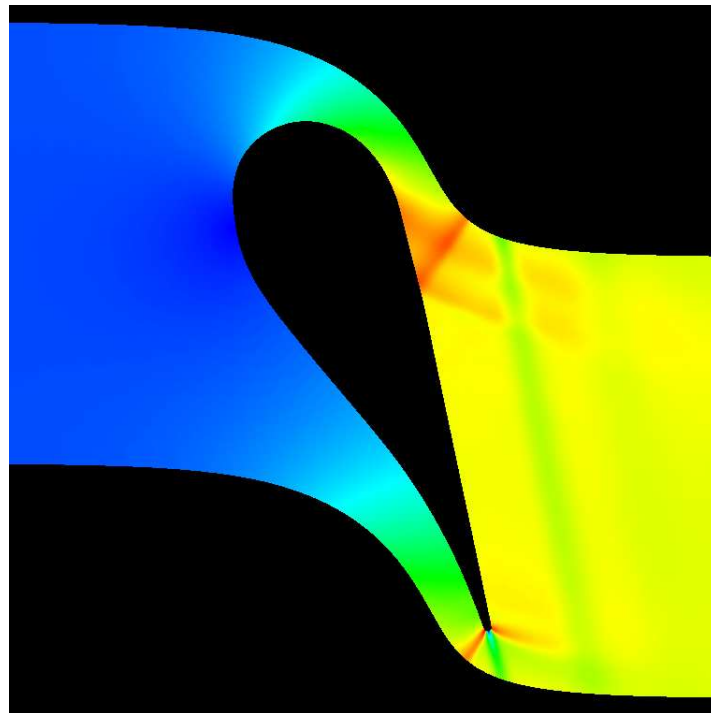


(b) DG

Figure 4-4: MISES and DG Mach contours (nominal).

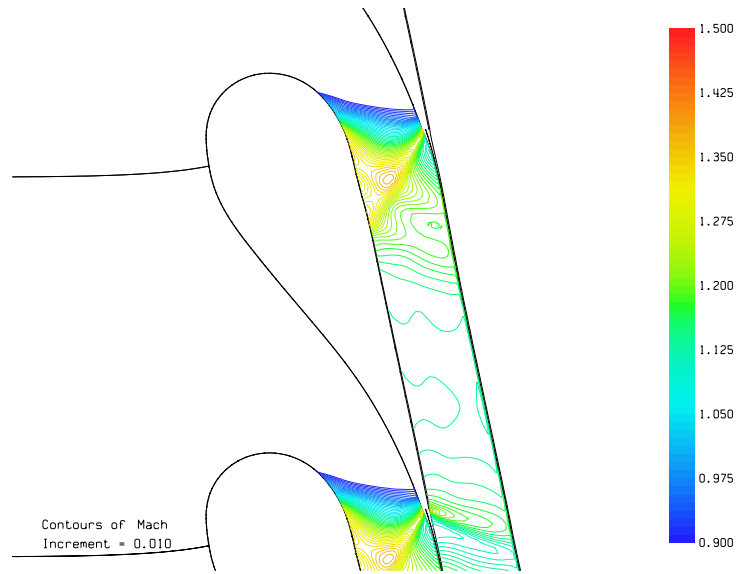


(a) MISES

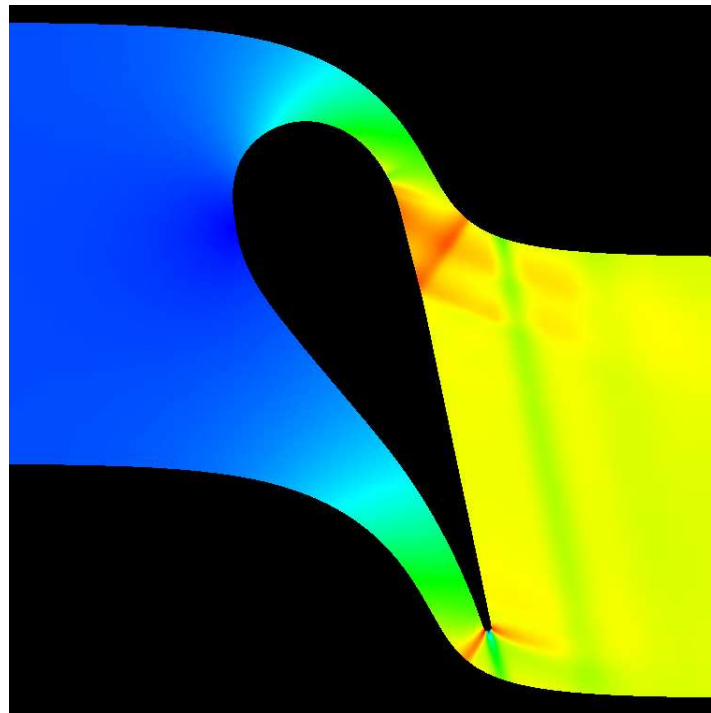


(b) DG

Figure 4-5: MISES and DG Mach contours. (node 2 perturbed)



(a) MISES



(b) DG

Figure 4-6: MISES and DG Mach contours (node 68 perturbed).

Chapter 5

Summary and Conclusions

This work shows the marked effect that manufacturing variability can have on the performance of a transonic turbine vane. Shape changes not only induce scatter in performance but also shift the distributions of shock-influenced quantities away from their nominal values. The results derived from Principal Components Analysis indicate that there is a significantly high probability that a manufactured vane will produce unacceptable values for flow rate and/or losses.

Virtually all of the differences in performance between the nominal vane and manufactured examples are due to geometry deviations in the region of sonic and supersonic flow. The flow is particularly sensitive to perturbations at the throat and trailing edge. The mechanisms that appear to drive this sensitivity are the opening/closing of the throat and the formation or modification of shocks. As a consequence, performance shows practically no sensitivity to shape changes upstream of the throat.

These results suggest the following recommendations to a manufacturer of transonic turbine vanes. Special care, such as additional or tighter tolerances, should be taken to make the throat area as close as possible to the design value; the trailing edge also requires particular attention. Controlling the shape variations at these locations as well as the suction side supersonic flow region may require more sophisticated manufacturing equipment, depending on the producer's current capabilities. The limited extent of the sensitive areas does nothing to defray the monetary costs of such ma-

chinery, but if enhanced accuracy and precision result in a slower process, time can be saved by only using it at and downstream of the throat. Fidelity to the design and shape smoothness are much more important in that area than elsewhere. Additionally and perhaps more usefully, it should not be necessary for aerodynamic reasons to scrap a vane that does not conform to the local deviation tolerance upstream of the throat so long as the basic shape is preserved. Each scrapped component represents a loss of time and money, and this research shows that imperfections over much of a vane's surface will not have appreciable effects on its performance.

5.1 Suggestions for Future Work

A work of this scope inevitably leaves much still to be done. The data used in the Principal Components Analysis is limited in size and extent. A larger population of Type I vanes will lead to higher-fidelity modeling of the geometric variability that arises during manufacturing. The vane measurements are from one phase of the production process only; it is worthwhile to investigate how shape variability changes over the course of the process. Data on the Type II vane is limited as well: its pre-production status prevents characterization of its mean shape deviation. It has the additional consequence that no gill slot is present, precluding the application of variability near the trailing edge. Since that feature has a high degree of influence on the flow, its irregularity should be included for a more accurate assessment of the performance distribution.

In addition to improving this work's data, one can also expand upon its analysis. It should be pointed out that doing any of these will require a non-trivial amount of time and/or computational resources. Geometry perturbation modes of different extent or type could be applied to see how those variables impact sensitivity. Linear sensitivity can be further explored by examining the effects of linear combinations of the local sensitivities. Viscous DG results would provide a check on the sensitivity derivative magnitudes. Manufacturing variability and sensitivity could be investigated over more

of the vane by including additional airfoil sections. The nonlinear sensitivity analysis, herein limited to a handful of locations on the vane, could reveal more if performed over the rest of the vane or at least the sensitive region. This research effort considers one vane at a time, but of course an actual engine has an entire row of different vanes. It will be fruitful to explore the engine-level effects of variability by carrying out the analysis presented here on groups of vanes and eventually an entire vane row.

Bibliography

- [1] “Gas Viscosity Calculator.” LMNO Engineering, Research, and Software, Ltd., 2003. <http://lmnoeng.com/Flow/GasViscosity.htm>.
- [2] “ProjectX User’s Guide.” MIT Aerospace Computational Design Laboratory, November 2007.
- [3] Barter, G. Personal communication, 2008.
- [4] Barter, G. *Shock Capturing with PDE-Based Artificial Viscosity for an Adaptive, Higher-Order Discontinuous Galerkin Finite Element Method*. Phd thesis, Massachusetts Institute of Technology, Department of Aeronautics and Astronautics, May 2008.
- [5] Bui-Thanh, T., Damodaran, M., and Willcox, K. “Inverse Airfoil Design Using Proper Orthogonal Decomposition on Computed Flowfield Snapshots.” SMA Connect Issue 3, Singapore-MIT Alliance, October 2004.
- [6] Couldrick, J. S. *A study of swept and unswept normal shock wave/turbulent boundary layer interaction and control by piezoelectric flap actuation*. Phd thesis, University of New South Wales, School of Aerospace, Civil and Mechanical Engineering, July 2006.
- [7] Denton, J. and Xu, L. “The trailing edge loss of transonic turbine blades.” ASME Paper 89-GT-326, 1989.
- [8] Drela, M. Personal communication, 2008.
- [9] Drela, M. and Youngren, H. “A User’s Guide to MISES 2.63.” MIT Aerospace Computational Design Laboratory, February 2008.
- [10] Fidkowski, K. “A High-order Discontinuous Galerkin Multigrid Solver for Aerodynamic Applications.” Master’s thesis, Massachusetts Institute of Technology, Department of Aeronautics and Astronautics, June 2004.
- [11] Fidkowski, K. J., Oliver, T. A., Lu, J., and Darmofal, D. L. “ p -Multigrid Solution of High-Order Discontinuous Galerkin Discretizations of the Compressible Navier-Stokes Equations.” *Journal of Computational Physics*, 207(1):92–113, 2005.

- [12] Garzon, V. E. *Probabilistic Aerothermal Design of Compressor Airfoils*. Phd thesis, Massachusetts Institute of Technology, Department of Aeronautics and Astronautics, February 2003.
- [13] Garzon, V. E. and Darmofal, D. L. “Impact of geometric variability on axial compressor performance.” *ASME Journal of Turbomachinery*, 125(4):692–703, October 2003.
- [14] Gegg, S. G. Personal communication, 2008.
- [15] Hicks, M. and Henne, P. A. “Wing design by numerical optimization.” *Journal of Aircraft* 7, 1978.
- [16] Kerrebrock, J. L. *Aircraft Engines and Gas Turbines*. MIT Press, Cambridge, MA, 1992.
- [17] Kim, S., Jameson, A., and Alonso, J. J. “Design Optimization of High-Lift Configurations Using a Viscous Continuous Adjoint Method.” AIAA Paper 2002-0844, January 2002.
- [18] Koff, B. L. “Gas turbine technology evolution - a designers perspective.” AIAA Paper 2003-2722, July 2003.
- [19] Lamb, C. M. “Probabilistic Performance-Based Geometric Tolerancing of Compressor Blades.” Master’s thesis, Massachusetts Institute of Technology, Department of Aeronautics and Astronautics, March 2005.
- [20] Miller, R. and Denton, J. “Loss Mechanisms in Turbomachines: Part 2, Loss generation in turbomachines.” Whittle Laboratory, Cambridge University, 2004.
- [21] Modisette, J. Personal communication, 2008.
- [22] Oliver, T. “Multigrid Solution for High-Order Discontinuous Galerkin Discretizations of the Compressible Navier-Stokes Equations.” Master’s thesis, Massachusetts Institute of Technology, Department of Aeronautics and Astronautics, August 2004.
- [23] Saad, M. A. *Compressible Fluid Flow*. Prentice Hall, Upper Saddle River, NJ, second edition, 1993.
- [24] Sheskin, D. *Handbook of parametric and nonparametric statistical procedures*. Chapman & Hall/CRC, Boca Raton, FL, fourth edition, 2007.
- [25] Sidwell, C. *On the Impact of Variability and Assembly on Turbine Blade Cooling Flow and Oxidation Life*. Phd thesis, Massachusetts Institute of Technology, Department of Aeronautics and Astronautics, June 2004.

- [26] Toal, D. J., Bressloff, N. W., , and Keane, A. J. “Kriging Hyperparameter Tuning Strategies.” University of Southampton, September 2007.
- [27] Walpole, R. E., Myers, R. H., Myers, S. L., and Ye, K. *Probability & Statistics for Engineers & Scientists*. Prentice Hall, Upper Saddle River, NJ, seventh edition, 2002.